공학석사학위논문

차량 후방형상 최적설계와 공력저감장치를 통한 초저공력차량 연구

Study on Ultra-Low Aerodynamic Drag Vehicle through Optimization of Rear Shape and Aerodynamic Drag Reduction Devices

2015년 2월

서울대학교 대학원

기계항공공학부

최 원 석

차량 후방형상 최적설계와 공력저감장치를 통한 초저공력차량 연구

Study on Ultra-Low Aerodynamic Drag Vehicle through Optimization of Rear Shape and Aerodynamic Drag Reduction Devices

지도교수 김 규 홍

이 논문을 공학석사 학위논문으로 제출함

2014년 10월

서울대학교 대학원

기계항공공학부

최 원 석

최원석의 공학석사 학위논문을 인준함

2014년 12월

위 원 장 _____

부위원장 _____

위 원 _____

Abstract

Study on Ultra-Low Aerodynamic Drag Vehicle through Optimization of Rear Shape and Aerodynamic Drag Reduction Devices

Choi. Wonseok
School of Mechanical and Aerospace Engineering
The Graduate School
Seoul National University

In this study, design of ultra-low aerodynamic drag vehicle was performed through optimization of rear shape and aerodynamic drag reduction devices. Sedan type vehicle was selected as a base model, which is being manufactured in these days. To reduce the aerodynamic drag, its rear shape was redesigned to square back type which is widely known as having low aerodynamic drag. Square back shape was designed by considering only the aerodynamic perspective. As a result, the aerodynamic drag was reduced. In order to minimize the aerodynamic drag of redesigned square back vehicle, optimization was performed. Roof angle, side angle and diffuser angle, which are the component of square back shape, were selected as the design variables. As a result of optimization, aerodynamic drag was decreased by 10.85% compared to initial square back shape. The relation between design variables and aerodynamic drag, together with the aerodynamic characteristics were obtained. Aerodynamic drag of optimal design was

reduced by 29.25% compared to sedan type vehicle. To additionally reduce the aerodynamic drag, aerodynamic drag reduction devices(side air dam, under deflector, wheel arch cover) were installed to optimal design of square back type vehicle. As a result of installing aerodynamic drag reduction devices, aerodynamic drag was improved by 33.15% compared to sedan type vehicle.

Keywords : Computational Fluid Dynamics, C.F.D, Aerodynamic Drag, Aerodynamic Drag Reduction Devices, Square Back Vehicle, Rear Shape Optimization

Student Number : 2013-20722

Table of Contents

List of Figures

List of Tables

1. Indroduction

1.1 Research Background

An interest having good fuel economy of vehicles has been increased due to high oil price, restriction on global CO2 emissions and restriction on fuel consumption demanding advanced technology and creating market entry barrier[1]. Thus, various studies have been performed, including variations in fuel economy of contemporary vehicles in accordance with the measurement methods of fuel consumption to correlation between fuel economy of vehicles and CO2 emissions[1-3]. Generally, 10% lighter body of the vehicles improves the fuel economy by approximately 3.2% and reduces the CO2 emissions by approximately 3.22% and 10% increased aerodynamic within 0.3 CD of the front and rear vehicle improves the fuel economy by approximately 2%. Furthermore, Drag distribution of vehicle is composed of rolling resistance, aerodynamic drag, weight, gearbox/drive train, etc.; the ratio of aerodynamic drag is 40% (shown as Figure 1-3). The aerodynamic drag is classified by detail items such as form drag, resistance by protruded structure, cooling drag, skin friction drag, and induced drag, as shown the Table 1-1[1, 17].

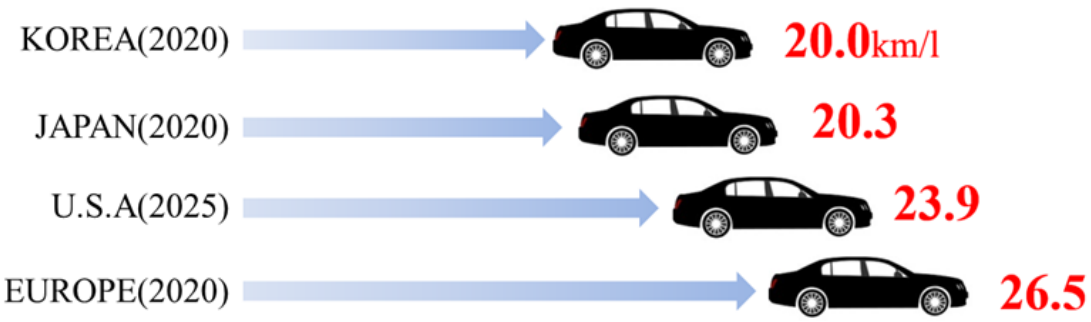

Figure 1-1. Fuel efficiency regulation of vehicle

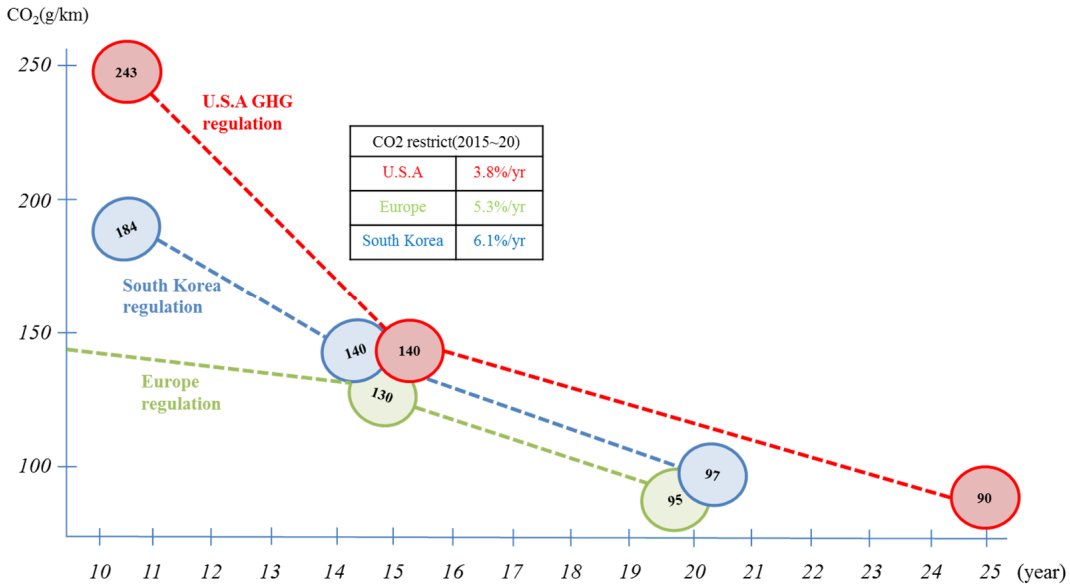

Figure 1-2. Trend of worldwide countries CO_2 restriction

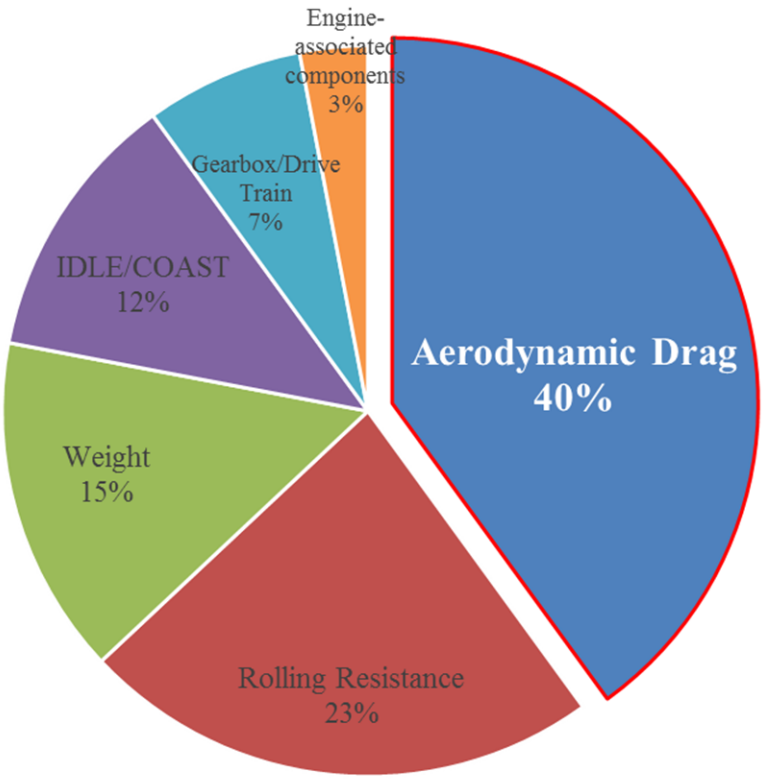

Figure 1-3. Drag distribution of road vehicles

Table 1-1. The general composition of aerodynamic drag from road vehicles

Category	Contribution Rate[%]
Vehicle Body	40~45%
Wheels and Housing	30~35%
Underbody	15~20%
Engine Cooling	5~10%
Rear View Mirrors	3~5%

1.1.1 Analysis on Affecting Factor for Aerodynamic Drag of Vehicle and Optimization for Low Aerodynamic Drag Vehicle

Analysis researches on contributing factors for aerodynamic drag reduction of vehicles and optimum design researches on optimum design for aerodynamic drag reduction were performed as following: First of all, Hyundai and Kia Motors, complete vehicle manufacturing companies, studied the affecting factors for aerodynamic drag of vehicle[4]; academic researches such as respective C_D result of various vehicle shapes in accordance with shape change of bonnet windshield, a-pillar, roof, and c-pillar were performed by Song et al.[5]; shape change of aerodynamic (C_D) in accordance with interference of side mirror, wheel arch, and wheel on the basis of YF SONATA(sedan type)[20] were performed and claimed that the wheel had the biggest impact. Kim et al. performed a numerical study on aerodynamic effect of vehicles in accordance with the shape change of front air deflector and rear shape of sedan on the basis of SAE recommended shape[6]. Besides, as researches on the optimum aerodynamic design, Lee et al. examined the variation of C_D in accordance with the body height of airfoil-shaped electric vehicles with optimum aerodynamic design to maximize the driving distance of ultra-light electric vehicles[7]; Kwon et al. performed a numerical study on driving performance of vehicles influenced by a streamlined design of a high-speed long-distance bus, examining the variation of the mechanical resistance of the bus with varied degrees and installed spoiler in the rear[8]; and Hur et al. performed shape optimization to reduce the aerodynamic drag of sports cars[9]. However, design variables

of sedan vehicles were already optimized, so the researches for design optimization were rarely performed by auto makers and academic associates.

1.1.2 Analysis on Aerodynamic Characteristics of Vehicle and Effort for Aerodynamic Drag Reduction

Hyundai Mobis suggested the necessity of Active Air Flap(AAF) to solve the problem of fuel economy and engine room cooling through a study on development of Active Air Flap system to enhance the fuel economy[10] and calculated value of C_D and level of contribution for fuel economy in accordance with conditions and AAF opening and closing areas (top/bottom) under condition of constant speed and hill climbing and estimated contribution level of fuel economy in accordance with warm-up time reduction. Similarly, Kim et al. studied internal temperature in engine room in accordance with AAF operating mode and time and flow control through shape-improved AAF installed on the air inlet grille in the engine room[11-13], and then they actually manufactured accordingly. The control logic of AAF was also examined with the actually manufactured one[14], resulting efficient improvement in all modes of fuel economy under condition of optimized control on the basis of the control logic such as AAF, cooling water pump, condenser, and etc. Recently, GM Korea performed a study on inflow ratio and aerodynamic performance defining front opening of mini vehicle in style development stage using Kriging method[15], then it determined necessary ratio of inflow for engine cooling as applicable in the beginning stage of mini vehicle development, figured out variation of inflow ratio and aerodynamic performance in accordance

with varied area of front top/bottom opening, and suggested optimal design for style of front area. The results of these studies were actually applied to installation of AAF in electric vehicle of Chevrolet Spark EV, newly released by GM Korea[44], and prospective installation of AAF in YF Sonata, manufactured by Hyundai and Kia Motors[45].

Son et al. observed that wheel was the most influential factors through the study on the variation of aerodynamic(C_D) in accordance with interference of side mirror, wheel arch, and wheel on the basis of sedan shape (YF Sonata)[20]. Park et al. performed analysis of wind noise in accordance with the OSRVM (side mirror of vehicle) shape modification[21] and low wind noise of OSRVM shape[22] and study of optimal shape of OSRVM for enhancement of vehicle performance[23], performing numerical study of turbulence evaluation for side vehicle and relative experiment. In this study, pressure changes of side vehicle, wind noise values, flow characteristics, and aerodynamic of vehicles(C_D) were calculated in accordance with the OSRVM shape modification. Furthermore, aerodynamic drag reduction devices of side vehicles such as side skirt or side air dam, on the basis of trucks, reduced fuel consumption by approximately 5%, Nox emissions, and 800 gallons of annual fuel consumptions and more than 9 tons of greenhouse gas, being used alone or with other aerodynamic drag reduction devices, as reported by US Environmental Protection Agency[24]. Kim et al. performed shape parametric study of active aerodynamic drag reduction devices of side vehicles[25] and then actually developed aerodynamic drag reduction devices of side vehicles for aerodynamic drag reduction of vehicle.

The researches about wake analysis in accordance with rear body shape

modifications and development of flow control and aerodynamic drag reduction devices were performed as followings: Recently, Hyundai and Kia Motors performed the study on wake structure modification and aerodynamic performance reduction in accordance with body shape[26]. In this study, wake measurement and analysis, C_D and wake structure, rear/rear-side spoiler effect and analysis, and optimization of wake structure with application of wake structure of low resistant vehicles and under edge of rear bumper were performed in accordance with body shape modification (wagon/ hatchback, sedan, and coupe) in wind tunnel test with 1/4 scale model. Song et al. performed estimation of C_D value in accordance with rear body shape modification such as trunk kick-up (Θt Lt), trunk side (Θs Ls), and rear undercover (diffuser type, Θu Lu), and etc.[27-30]. Kang et al. showed that more angular and flat trunk reduced down-wash (COANDA effect) and induced drag through the study of COANDA effect at trunk of vehicle[31]. Moreover, it showed why total C_D was reduced in consideration of rotating wheel and moving ground effect and that as the under body was simpler and the ground moved faster, the flow speed of under body became faster, reducing COANDA effect and then reduced the induced drag, having effect of total C_D reduction[32, 33].

According to the evaluation study performed by Lai et al. in the late of 2000 of effect of the outlet flow from the engine room on the aerodynamic performance[16], the fact that underflow of a vehicle largely influenced total aerodynamic drag and the total aerodynamic drag was determined by the momentum recovery from the outlet flow of the engine room was observed by wind tunnel measurements. And horizontal air exhaust was installed at the front-end area in the engine room; full-undercover was recommended as

the best way.

Beyond the rear body shape modification, more researches were in progress, pursuing to actively control the wake of vehicle. The researches about these active flow controls of rear vehicle and development of active aerodynamic drag reduction device were performed as followings: Park et al. performed studies on C_D reduction due to installation of synthetic jet in the rear body under condition of 1/4 scale model of sedan[34], shape optimization study of Piezo-actuated synthetic jet[35], and study on aerodynamic drag reduction of simplified bluff shape or just simplified shape of vehicle using synthetic jets[36-38]. For more active flow control, studies of rear shape change like rear diffuser and installation of flow control device were also in progress. Cho et al. showed that the operating speed of vehicle was 80~120 kph with the biggest mean of aerodynamic performance when the length of rear diffuser was 400mm[39]; Kang et al. suggested the maximum performance shape of rear diffuser after calculating the maximum performance length 450mm of the rear diffuser in the range of 70~160 kph of vehicle operating performance[40~42]. Furthermore, Kim et al. showed the periodicity of C_D in accordance with the length of rear diffuser at specific speed and performed evaluation of the prototype of rear diffuser shape[43]. Kim et al. performed shape parametric study applying Active Air Flap, undercover, under fin, side air dam, under deflector, and rear diffuser to sedan vehicles[45].

1.2 Research Objective

The purpose of this study is to reduce the aerodynamic drag for driving vehicle. In order to decrease the aerodynamic drag, rear shape of sedan type vehicle was redesigned to square back type. Redesigned rear shape was selected by baseline, and optimization was performed using variables which are judged as having more sensitivity. Through the optimization, optimal design and relation of variables and aerodynamic drag were found. Aerodynamic drag reduction devices were installed to optimal design, then drag aerodynamic drag was improved further.

2. Physical Modeling and Numerical Methods

2.1 Physical Modeling

2.1.1 Governing Equations

To evaluate the thermal and flow field in engine room, this study used incompressible Navier-Stokes equations, energy equation, and k-ε wall function turbulence models[46, 47].

The steady and compressible Navier-Stokes equation could be expressed as non-dimensionalized conservation form of vector type on the 3-dimentional x, y, and z orthogonal coordinates system, as shown below:

$$\frac{\partial Q^*}{\partial t^*}+\frac{\partial E^*}{\partial x^*}+\frac{\partial F^*}{\partial y^*}+\frac{\partial G^*}{\partial z^*}=\frac{\partial E_v^*}{\partial x^*}+\frac{\partial F_v^*}{\partial y^*}+\frac{\partial G_v^*}{\partial z^*}$$

Here, conservation variable, Q and flux vectors, E, F, E_v, F_v can be defined as below :

$$Q^*=\begin{bmatrix}\rho^*\\ \rho^* u^*\\ \rho^* v^*\\ \rho^* w^*\\ \rho^* e_t^*\end{bmatrix},\ E^*=\begin{bmatrix}\rho^* u^*\\ \rho^* u^{*2}+p^*\\ \rho^* u^* v^*\\ \rho^* u^* w^*\\ (\rho^* e_t^*+p^*)u^*\end{bmatrix},\ E_v^*=\begin{bmatrix}0\\ \tau_{xx}^*\\ \tau_{xy}^*\\ \tau_{xz}^*\\ u^*\tau_{xx}^*+v^*\tau_{xy}^*+w^*\tau_{xz}^*-q_x^*\end{bmatrix},$$

$$F^* = \begin{bmatrix} \rho^* v^* \\ \rho^* v^* u^* \\ \rho^* v^{*2} + p^* \\ \rho^* v^* w^* \\ (\rho^* e_t^* + p^*) v^* \end{bmatrix}, \quad F_v^* = \begin{bmatrix} 0 \\ \tau_{yx}^* \\ \tau_{yy}^* \\ \tau_{yz}^* \\ u^* \tau_{yx}^* + v^* \tau_{yy}^* + w^* \tau_{yz}^* - q_y^* \end{bmatrix},$$

$$G^* = \begin{bmatrix} \rho^* w^* \\ \rho^* w^* u^* \\ \rho^* w^* v^* \\ \rho^* w^{*2} + p^* \\ (\rho^* e_t^* + p^*) w^* \end{bmatrix}, \quad G_v^* = \begin{bmatrix} 0 \\ \tau_{zx}^* \\ \tau_{zy}^* \\ \tau_{zz}^* \\ u^* \tau_{zx}^* + v^* \tau_{zy}^* + w^* \tau_{zz}^* - q_z^* \end{bmatrix}$$

$$\tau_{xx}^* = \frac{1}{Re_\infty}[2\mu^* \frac{\partial u^*}{\partial x^*} + \lambda^* \nabla^* \cdot \overrightarrow{V^*}], \quad \tau_{xy}^* = \tau_{yx}^* = \frac{1}{Re_\infty}[\mu^* (\frac{\partial u^*}{\partial y^*} + \frac{\partial v^*}{\partial x^*})],$$

$$\tau_{xz}^* = \tau_{zx}^* = \frac{1}{Re_\infty}[\mu^* (\frac{\partial w^*}{\partial x^*} + \frac{\partial u^*}{\partial z^*})], \quad \tau_{yy}^* = \frac{1}{Re_\infty}[2\mu^* \frac{\partial v^*}{\partial y^*} + \lambda^* \nabla^* \cdot \overrightarrow{V^*}],$$

$$\tau_{yz}^* = \tau_{zy}^* = \frac{1}{Re_\infty}[\mu^* (\frac{\partial v^*}{\partial z^*} + \frac{\partial w^*}{\partial y^*})], \quad \tau_{zz}^* = \frac{1}{Re_\infty}[2\mu^* \frac{\partial w^*}{\partial z^*} + \lambda^* \nabla^* \cdot \overrightarrow{V^*}],$$

$$q_x^* = -\frac{\mu^*}{Re_\infty \mathrm{Pr}(\gamma-1)M_\infty^2} \frac{\partial T^*}{\partial x^*}, \quad q_y^* = -\frac{\mu^*}{Re_\infty \mathrm{Pr}(\gamma-1)M_\infty^2} \frac{\partial T^*}{\partial y^*},$$

$$q_z^* = -\frac{\mu^*}{Re_\infty \mathrm{Pr}(\gamma-1)M_\infty^2} \frac{\partial T^*}{\partial z^*}$$

Since this study used incompressible Navier-Stokes equations, density of all terms were calculated by ρ = constant.

2.1.2 Turbulence Model

In this study, standard $k-\epsilon$ model was used as turbulence model. The

standard $k-\epsilon$ model is a model based on model transport equations for the turbulence kinetic energy(k) and its dissipation rate(ϵ). The model transport equation for k is derived from the exact equation, while the model transport equation for ϵ was obtained using physical reasoning and bears little resemblance to its mathematically exact counterpart.

In the derivation of the standard $k-\epsilon$ model, the assumption is that the flow is fully turbulent, and the effects of molecular viscosity are negligible. The standard $k-\epsilon$ model is therefore valid only for fully turbulent flows.

The turbulence kinetic energy, k, and its rate of dissipation, ϵ, are obtianed from the following transport equations.

$$\frac{\partial}{\partial t}(\rho k)+\frac{\partial}{\partial x_i}(\rho u_i k-\frac{\mu_t}{\sigma_k}\frac{\partial k}{\partial x_i}) = -\rho\varepsilon+G_k+\frac{\partial}{\partial x_i}(\mu\frac{\partial k}{\partial x_i})$$

and

$$\frac{\partial}{\partial t}(\rho\varepsilon)+\frac{\partial}{\partial x_i}(\rho u_i\varepsilon-\frac{\mu_t}{\sigma_\varepsilon}\frac{\partial \varepsilon}{\partial x_i}) = \frac{\partial}{\partial x_i}(\mu\frac{\partial \varepsilon}{\partial x_i})-C_{1\varepsilon}\frac{\varepsilon}{k}G_k-C_{2\varepsilon}\rho\frac{\varepsilon^2}{k}$$

The model constants used in this study were shown in the Table 2-1.

Table 2-1. Modeling Constants Used in the Turbulence Model

$C_{1\epsilon}$	$C_{2\epsilon}$	C_μ	σ_k	σ_ϵ
1.44	1.92	0.09	1.0	1.3

2.2 Numerical Methods

2.2.1 Spatial Discretization

In this study, the spatial discretization was higher than second-order accuracy for calculation accuracy. Using MPI(Message Passing Interface), parallel computation with 64 CPU was performed; implicit solution was applied to the parallel computation in repeated calculation process[48-53]. Since incompressible a Navier-Stokes equation was used, it was assumed that all terms had equivalent density.

Navier-Stokes equation is defined as non-linear PDE, which stands for Partial Differential Equation, as well as hyperbolic type equation with respect to time. To solve numerically the flow field that we interested in, it is required for the equation as mentioned above to be converted into an algebraic equation using the method for not only time discretization but spatial discretization. When the governing equation is rearranged in terms of implicit method after applying finite volume method to it, the equation will be formulated in the following as proposed by MacCormack.

$$\{Nmerics\}\delta Q = \{Physics\}$$

Here, δQ is corrected in each time step, and $\{Physics\}$, the right side is in term of discretizating the equation and related to the accuracy of numerical solution, $\{Nmerics\}$ has a role of passing the value of each time step to the next time step, and affect the efficiency of the calculation affects.

Upwind difference method, which is based on Osher's Flux Difference Splitting scheme, was used to calculate inviscid flux in the right hand side. In addition, central differencing method, which is well known that it usually uses 2nd accuracy, was used to calculate viscous flux.

2.2.2 Upwind Differencing Based on Osher's FDS

Upwind difference, which is based on FDS method by Osher, was used to discretize convective flux in space. A numerical dissipation term is added to inviscid term, and hence it will be shown in the following.

$$\mathcal{E}_{i+1/2} = \frac{1}{2}\left(\mathcal{E}_{i+1} + \mathcal{E}_{i}\right) - \mathcal{D}_{i+1/2}$$

Here, $\mathcal{D}_{i+1/2}$ can be described as shown below having 1st order accuracy.

$$\mathcal{D}_{i+1/2} = \frac{1}{2}\left(\Delta\ \mathcal{E}_{i+1/2}^{+} - \Delta\ \mathcal{E}_{i+1/2}^{-}\right)$$

$\Delta\ \mathcal{E}^{\pm}$ stands for the flux that coming and going toward the direction of positive and negative on the central of i+1/2.

$$\Delta\ \mathcal{E}_{i+1/2}^{\pm} = \mathcal{A}^{\pm}(\overline{Q})\,\Delta Q_{i+1/2}$$

$\overline{Q}$ stands for average value between both sides at which flux would be

estimated.

$$\overline{Q} = \frac{Q_{i+1} + Q_i}{2}$$

ΔQ is as shown below.

$$\Delta Q_{i+1/2} = Q_{i+1} - Q_i$$

$\hat{A}^{\pm}$, which stands for positive and negative Jacobian matrix, can be obtained by similarity transformation. The similarity transformation is as shown below.

$$\hat{A}_i = X_i \Lambda_i X_i^{-1}$$

General flux vector can be described as shown below,

$$\hat{E}_i = \frac{1}{J}\begin{bmatrix} \beta W \\ k_t u + k_x p + u W \\ k_t v + k_y p + v W \end{bmatrix}$$

The value of matric is as shown below as i=1,2 which makes $\hat{E}_i = \hat{E}, \hat{F}$

$$k_x = \frac{1}{J}\frac{\partial \xi_i}{\partial x}, \quad i = 1, 2$$

$$k_y = \frac{1}{J}\frac{\partial \xi_i}{\partial y}, \quad i = 1, 2$$

$$k_t = \frac{1}{J}\frac{\partial \xi_i}{\partial t}, \quad i = 1, 2$$

A contravariant velocity(W) is as shown below.

$$W = k_x u + k_y v$$

Then, Jacobian Matrix can be tabulated as shown below.

$$\hat{A}_i = \frac{\partial E_i}{\partial Q}\begin{bmatrix} 0 & k_x\beta & k_y\beta \\ k_x & k_x u + W + k_t & k_y u \\ k_y & k_x v & k_y v + W + k_t \end{bmatrix}$$

Applying similarity transformation, then we have,

$$\Lambda_i = diag[\lambda_1, \lambda_2, \lambda_3]$$

$$\lambda_1 = W + k_t$$

$$\lambda_2 = W + k_t$$

$$\lambda_3 = W + \frac{k_t}{2} + c$$

c stands for artificial speed of sound.

$$c = \sqrt{(W + \frac{k_t}{2})^2 + \beta(k_x^2 + k_y^2)}$$

Using above equation, it can be solved right eigenvector as well as its inverse matrix.

$$X_i = \frac{1}{2\beta c(c^2 - 0.25k_t^2)} \begin{bmatrix} 0 & \beta(c^2 - 0.25k_t^2) & -\beta(c^2 - 0.25k_t^2) \\ -2\beta c k_y & (u\lambda_2 + \beta k_x)(c + 0.5k_t) & (u\lambda_3 + \beta k_x)(c + 0.5k_t) \\ 2\beta c k_x & (v\lambda_2 + \beta k_y)(c + 0.5k_t) & (v\lambda_3 + \beta k_y)(c + 0.5k_t) \end{bmatrix}$$

$$X_i^{-1} = \begin{bmatrix} k_y u - k_x v & -v\lambda_1 - \beta k_y & u\lambda_1 + \beta k_x \\ -\lambda_3 & \beta k_x & \beta k_y \\ -\lambda_2 & \beta k_x & \beta k_y \end{bmatrix}$$

Diagonal matrix, Λ_i can be categorized in the characteristics of both positive and negative.

$$|\Lambda_i| = diag[\,|\lambda_1|, |\lambda_2|, |\lambda_3|\,]$$

$$\Lambda_i = \Lambda_i^+ + \Lambda_i^-$$

$$\Lambda_i^+ = \frac{\Lambda_i + |\Lambda_i|}{2}$$

$$\Lambda_i^- = \frac{\Lambda_i - |\Lambda_i|}{2}$$

Using diagonal matrix, Λ_i decomposed to positive and negative things from Jacobian Matrix, $\mathcal{A}_i$,

$$\mathcal{A}_i = X_i(\Lambda_i^+ + \Lambda_i^-)X_i^{-1}$$

$$= X_i \Lambda_i^+ X_i^{-1} + X_i \Lambda_i^- X_i^{-1} = \mathcal{A}_i^+ + \mathcal{A}_i^-$$

Estimating the absolute value of Jacobian matrix,

$$|\mathcal{A}_i| = X_i|\Lambda_i|X_i^{-1}$$
$$= \mathcal{A}_i^{+} - \mathcal{A}_i^{-}$$

Rearrange the $\mathcal{D}_{i+1/2}$ term, we have,

$$\mathcal{D}_{i+1/2} = \frac{1}{2}|\mathcal{A}_i|(Q_{i+1} - Q_1)$$

2.2.3 Time Integration

The governing equation considered time interval will be shown as below.

$$\frac{1}{J}\frac{\partial Q^{n+1}}{\partial t} + \left(\frac{\partial \hat{E}}{\partial \xi} + \frac{\partial \hat{F}}{\partial \eta}\right)^{n+1} - \left(\frac{\partial \hat{E}_\nu}{\partial \xi} + \frac{\partial \hat{F}_\nu}{\partial \eta}\right)^{n+1} = S_g^{n+1} + S_\sigma^{n+1}$$

Using Taylor series expansion in respect to time level n, the equation is:

$$\mathcal{E}^{n+1} = \mathcal{E}^n + \left[\frac{\partial \mathcal{E}}{\partial Q}\right]\Delta Q + o(\Delta t^2) \cong \mathcal{E}^n + \mathcal{A}\Delta Q$$

By similar way, F can be tabulated in the following.

$$\mathcal{F}^{n+1} \cong \mathcal{F}^n + \mathcal{B}\Delta Q$$

Inviscid flux can be simply tabulated as shown below.

$$E_v^{n+1} \cong E_v^n$$

$$F_v^{n+1} \cong F_v^n$$

Using above relation, the governing equation is rearranged in the following.

$$\frac{1}{J}\frac{\Delta Q}{\Delta t} + \frac{\partial}{\partial \xi}\left(\widehat{E}^n + \hat{A}\Delta Q\right) + \frac{\partial}{\partial \eta}\left(\widehat{F}^n + \hat{B}\Delta Q\right) - \left(\frac{\partial \widehat{E}_v}{\partial \xi} + \frac{\partial \widehat{F}_v}{\partial \eta}\right)^n = S_g + S_\sigma$$

Rearrange the equation, we have,

$$\frac{1}{J}\frac{\Delta Q}{\Delta t} + \frac{\partial}{\partial \xi}(A\Delta Q) + \frac{\partial}{\partial \eta}(B\Delta Q)$$
$$= -\left(\frac{\partial}{\partial \xi}(E - E_v) + \frac{\partial}{\partial \eta}(F - F_v) + \right)^n + S_g + S_\sigma$$
$$\left(\frac{I}{J\Delta t} + \frac{\partial A}{\partial \xi} + \frac{\partial B}{\partial \eta}\right)\Delta Q = -\left(\frac{\partial}{\partial \xi}(E - E_v) + \frac{\partial}{\partial \eta}(F - F_v)\right)^n$$
$$= -R^n + S_g + S_\sigma$$

Here, I = Indentity matrix / R = Residual term including viscous term. This can be categorized in the following as the characteristic value of flux Jacobian.

$$\left[\frac{I}{J\Delta t} + \delta_\xi^- A^+ + \delta_\xi^+ A^- + \delta_\eta^- B^+ + \delta_\eta^+ B^-\right]\Delta Q = -R^n + S_g + S_\sigma$$
$$= -R^n$$

2.2.3.1 Dual-Time Stepping

To figure out time-accurate in unsteady state problem, pseudo-time sub-iteration was used as the following formula:

$$\frac{1}{J}\frac{\partial Q}{\partial t} = -\mathcal{R}$$

To obtain second-order accuracy, 3 points were interpolated in the backward formula and transposed to the right hand side as followings:

$$0 = -\frac{1.5Q^{n+1} - 2Q^{n} + 0.5Q^{n-1}}{J\Delta t} - \mathcal{R}^{n+1}$$

Here, Δt : physical time step

Superscript n : property at $t = n\Delta t$

If differential equation in pseudo-time of Q is added to the left hand side, it was shown below:

$$\frac{1}{J}\frac{\partial Q^{n+1}}{\partial \tau} = -\mathcal{R}^{n+1} - \frac{1.5Q^{n+1} - 2Q^{n} + 0.5Q^{n-1}}{J\Delta t} = -\mathcal{R}^{n+1} - \mathcal{S}^{n+1}$$

Generally, since the first degree showed better performance of convergence than higher degree, differential equation in pseudo-time can be interpolated into the first degree of Eluer equation, as shown below.

$$\frac{Q^{n+1,\,m+1}-Q^{n+1,\,m}}{J\Delta\tau} = -\mathcal{R}^{n+1,\,m+1} - \mathcal{S}^{n+1,\,m+1}$$

Here, m showed pseudo-time iteration level. Time accuracy was necessarily considered in physical time rather than pseudo-time, thus the above formula obtained second-order time accuracy.

It can be rewritten as below:

$$\left[\frac{I}{J\Delta t}+\left(\frac{\partial \mathcal{R}}{\partial Q}+\frac{\partial \mathcal{S}}{\partial Q}\right)^{n+1,\,m}\right]\Delta Q_{n+1,\,m} = -\left(\mathcal{R}^{n+1,\,m}+\mathcal{S}^{n+1,\,m}\right)$$

$$Q=\frac{1}{J}[p,u,v]^T$$

$$I_{t\tau}=diag\left[\frac{1}{\Delta\tau},\frac{1.5}{\Delta t},\frac{1.5}{\Delta t}\right]$$

$$I_m=diag[0,1,1]$$

Here, $\hat{S}$: unsteady source-like term

To improve the convergence and stability, local time stepping method was used.

3. Design of Square Back Type Vehicle

3.1 Base Model

In this study, base model is YF-SONATA, a vehicle manufactured today by Hyundai Motors Company. Complex aerodynamic characteristic factors and variables regarding the vehicle's aerodynamic shape. Thus, detailed vehicle's 3-D model is very important for fluid analysis. Figure 4-1 shows 3-D detailed shape of the base model. The front part of the vehicle has radiator grills, engine room, headlights, and the side part of the vehicle has side mirrors. The rear part of the vehicle has rear indicator lights, and the detailed under part of vehicle is simulated. This vehicle exterior has thoughtfully considered for rotating wheel effects of driving condition.

In order to reduce the aerodynamic drag of YF-SONATA, some researches[18,19,25,43,45] about fluid analysis were performed and according to this study, base model's drag coefficient is 0.31012. Despite various research, sedan types of vehicles are faced with limitations of reducing aerodynamic drag. To overcome limitations and reduce drag even further, square back design has been applied to the rear of sedan type vehicle.

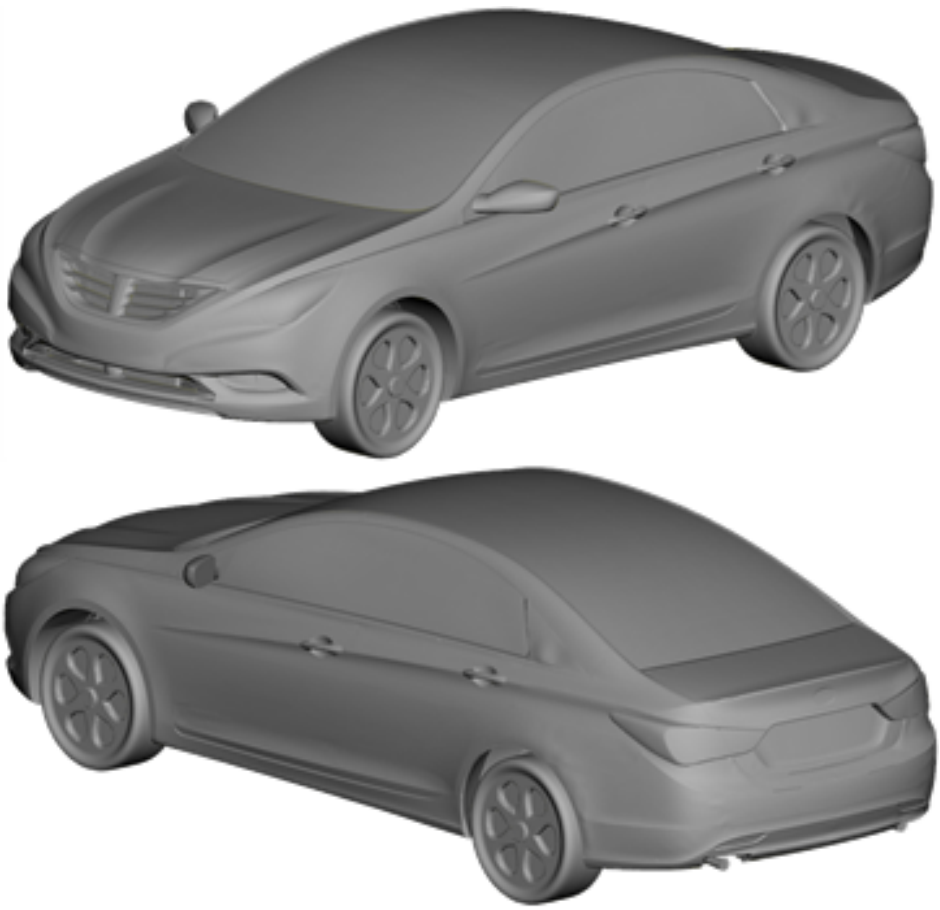

Figure 4-1. Shape of sedan type YF SONATA

3.2 Redesigning Rear Shape of Sedan Type to Square Back Type

The main reason for redesigning the sedans' rear shape to a square back design is to reduce aerodynamic drag. If there is no reduction of the aerodynamic drag after redesigning to the square back, then it is a design failure. The front part of the YF-SONATA retains the same design, but the rear part of the vehicle has been redesigned to a square back type. There are considerable factors involved in the square back design.

(1) The end of the vehicle's roof has been lowered compared to the maximum height of the roof with an installed diffuser at the end of the trunk. The implication of this design is that when air flows out of the rear end of the vehicle, the wake zone is reduced. The wake zone creates pressure drop at the rear of the vehicle. These air pressure differences between the front and rear are the main problematic factors of aerodynamic drag. Also, installing the diffuser at the end of the trunk will help to recover overall surface pressure. In general, there are no significant changes in reducing aerodynamic drag between the diffuser angle and length[54].

(2) Applying the camber design creates the "curvy" roof line. The stiff drop of the roof line will cause separation and it is the cause of the aerodynamic drag. The curvy roof line will act as an airfoil so that the flow of the air won't be separated on the roof surface.

(3) Installing “kick-up” at the end of the roof and the right angle shaped “side-end” will suppress induced drag from the COANDA effect. The COANDA effect is defined as the tendency of a fluid jet to be attracted to a nearby surface because of the viscosity of the air. If a certain amount of curvature is exists at the rear end of a vehicle as shown in Figure 4-2, the incoming air flows along the surface due to COANDA effect. In such a case, viscosity of the air results in the vehicle’s surface attracting the flow towards itself and as a reaction of such force, the flow attracts the surface of the vehicle resulting in right-upward force generated. The horizontal component of the generated force acts as induced drag which is a bad influence to the aerodynamic drag of the vehicle. Application of kick-up and right angle shaped “side-end” suppresses the generation of the induced drag.

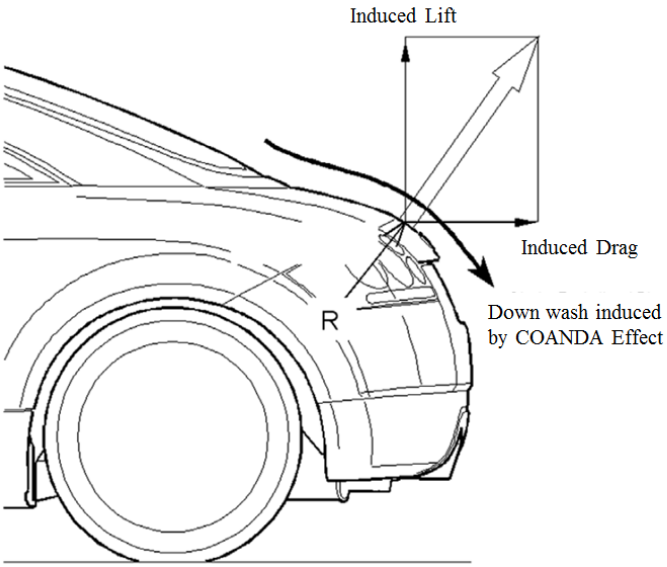

Figure 4-2. COANDA effect around rear body

(4) Installing rear view cameras instead of the side mirrors is done in order to reduce the aerodynamic drag. There is research[20] regarding the effects of the side mirror's aerodynamic drag. Replacing the side mirror with the rear cameras eliminates air drag. Drivers can monitor the situation outside of the vehicle. The design of the camera is a wedge shape in order to minimizing the air drag.

(5) In this study, and it was solely focused on the aerodynamic exterior, so a specially designed active air flap and full undercover were installed: Engine room and the under compartment were disregarded in this study. The radiator grill has been closed. There is considerable research regarding active air flap and full undercover design. A closed active air flap will prevent the air from flowing inside of the engine room, and a full undercover will smooth out the flow of air underneath of the vehicle. It was seen that active air flap blocks air entering the engine room which prevents generation of drag inside the engine room and undercover prevents complex flow generated due to underparts of vehicle, instead it makes the air to flow smoothly along the undersurface from previous researches[10,12,14,18,45]. In case of active air flap all closed of sedan type vehicle, aerodynamic drag was reduced by 4.4%[12], and full undercover reduced the drag by 4.1%[18].

Based on these considerations a square back design has been applied to the YF-SONATA. Figure 4-3 shows the shape of the square back type YF-SONATA. Figure 4-4 through 4-8 indicate these considerations.

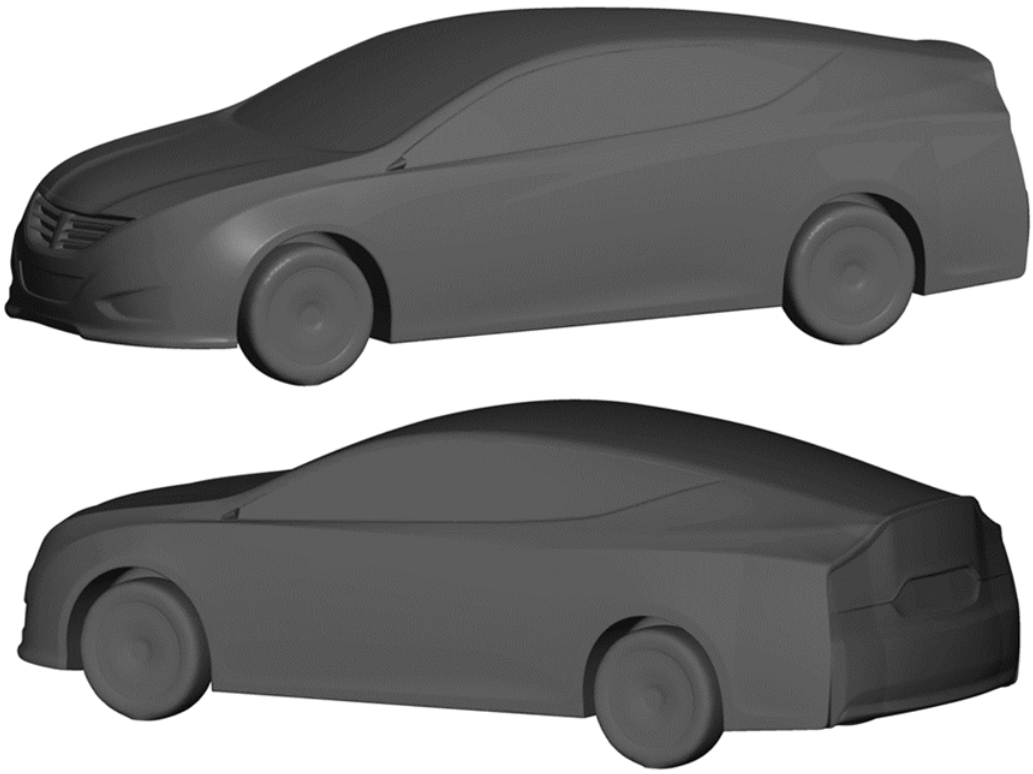

Figure 4-3. Shape of square back type YF SONATA

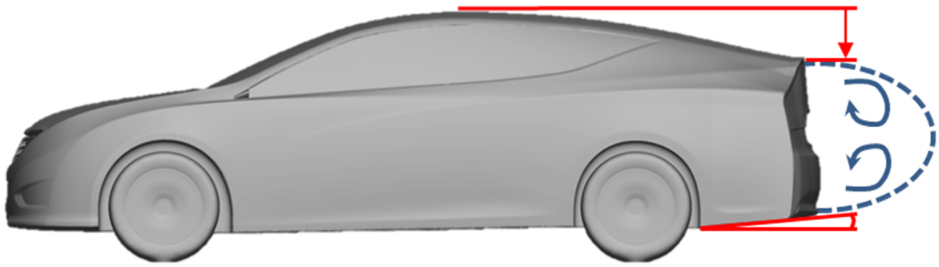

Figure 4-4. Consideration of reducing wake region of vehicle

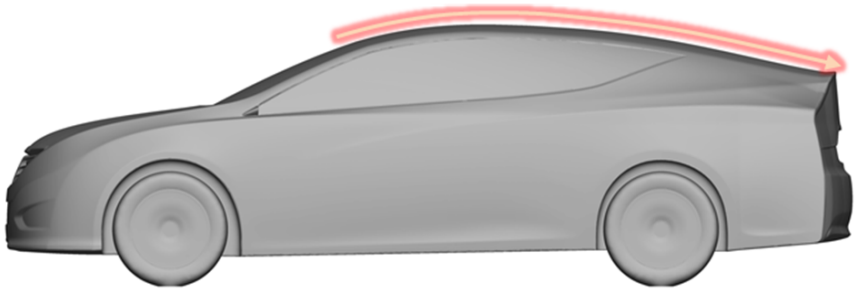

Figure 4-5. Roof applied airfoil camber

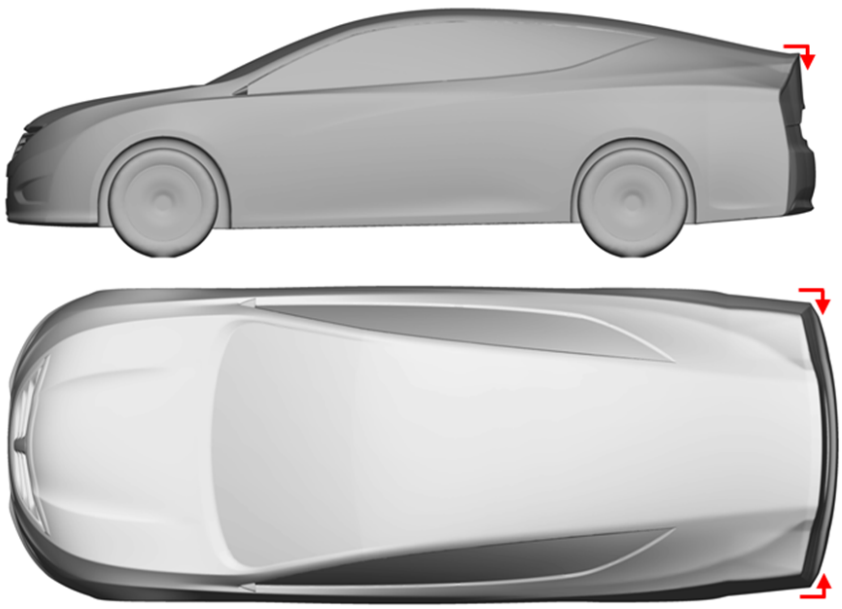

Figure 4-6. Kick up at end of roof and rectangular shape at end of vehicle side

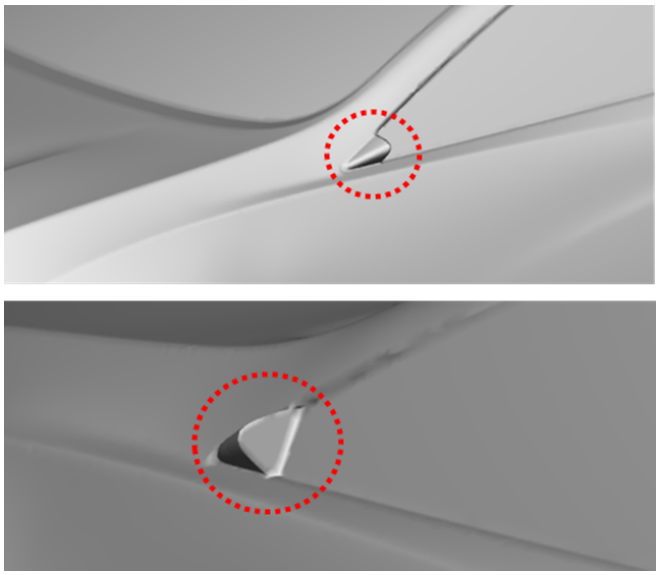

Figure 4-7. Rear view camera instead of side mirror

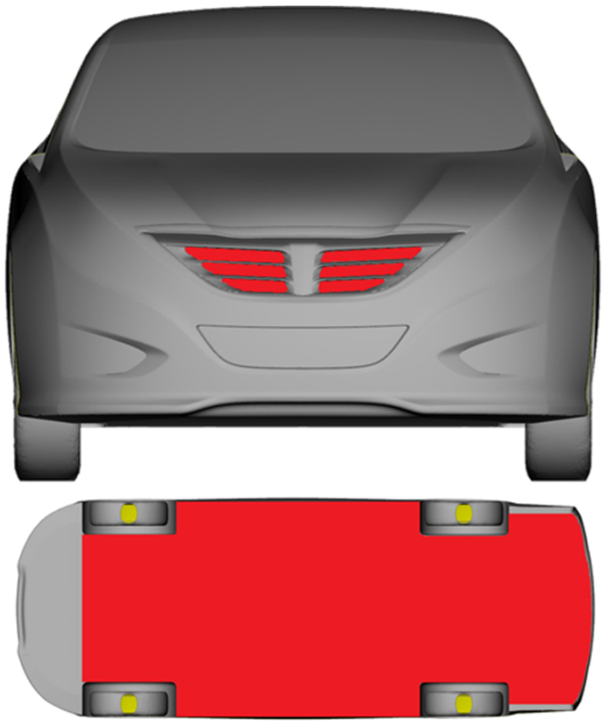

Figure 4-8. Installation of active air flap and full undercover

3.3 Flow Analysis

In this study, ANSYS Fluent ver13.0, a commercial tool, was used for the computational fluid analysis. Gambit ver2.4.6 and ANSA ver13.2.3 were used for 3D shape modeling and creation of surface grids. Volume grids were created by Tgrid ver13.0.

3.3.1 Grid Generation

Unstructured grids of surface and volume were created for flow analysis of external vehicle. Even though the number of grids was differentiated by analysis case, it was composed of approximately 10,000,000 ~ 11,000,000 of unstructured grids. Based on the vehicle scale of vehicle and maximum driving speed of the analysis cases, the height of turbulence boundary layer was 7.054 cm, and the height of prism layers were 8.249 cm, higher than the turbulence boundary layer. The shape of grid was shown in Figure 4-9.

3.3.2 Boundary Condition

Figure 4-10 shows boundary condition

(1) Boundary Condition of External Vehicle

The distance from the vehicle to the front and rear boundary were set by 10 times of vehicle length for analysis domain; and case of 10 times was chosen since the general pattern of wake could be observed. The front boundary was under condition of velocity inlet, and the rear

boundary was under condition of pressure outlet. The inflow velocity was set by 120 km/h(33.3333 m/s) as driving speed, and the temperature of fluid was applied by 30℃. Besides, symmetric condition was applied to the external boundary, removing interaction with flow. The surface temperature of the vehicle was set by 30 ℃, which as equivalent with the temperature of external flow[11,12].

(2) Boundary Condition Considering Driving Effect

To simulate actual driving effect of vehicle, the ground wall was applied to moving wall boundary to be moved at the same speed with the driving speed of the vehicle. Furthermore, to consider the wheel rotation effect due to rotating wheel of driving car, the wheel was under condition of rotating wall boundary to simulate the wheel actual rotation effect of vehicle[11,12].

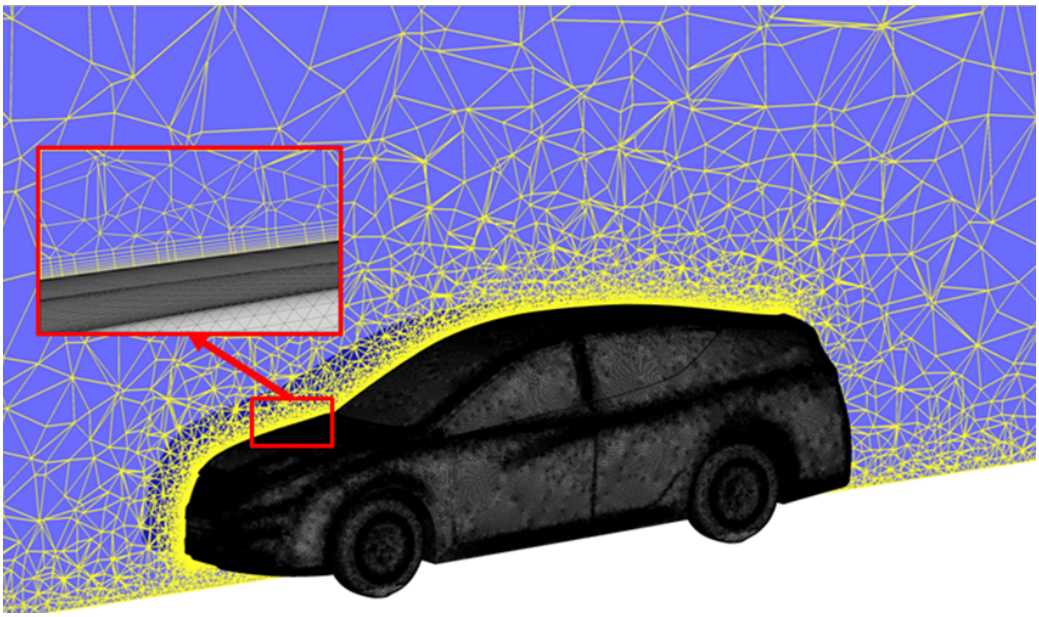

Figure 4-9. Grid composition of surface of vehicle and volume

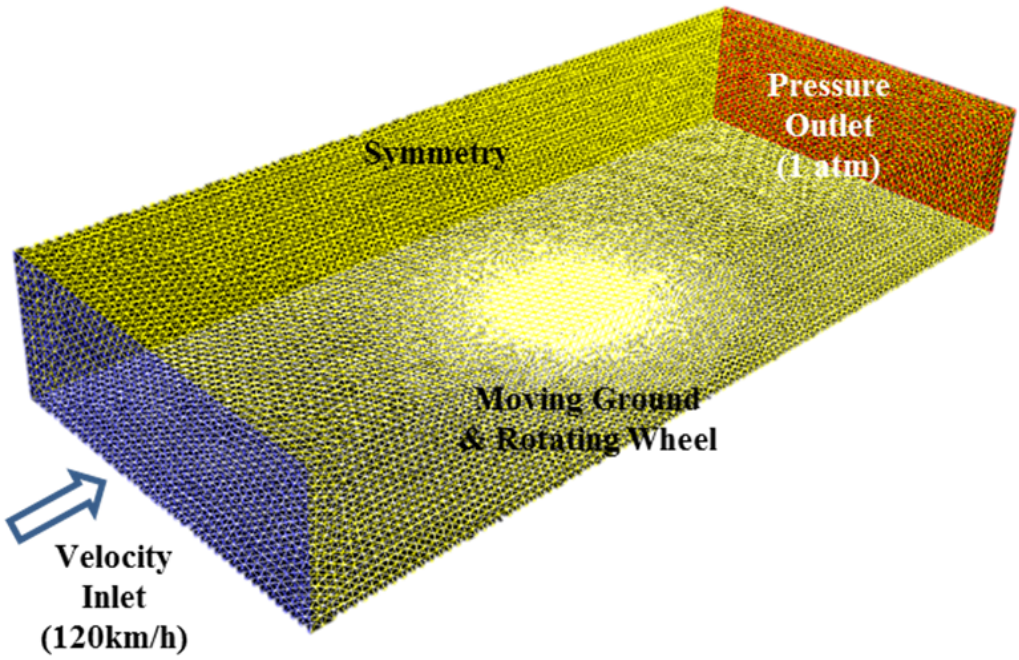

Figure 4-10. Boundary condition

3.3.3 Analysis Result

Generally, drag coefficient is shown below.

$$C_D = \frac{Drag\,Force}{\frac{1}{2}\rho V^2 A}$$

Drag is inclusive of viscous and pressure drag. Denominator of $\frac{1}{2}\rho V^2$ represents dynamic pressure and A represents the projection area of the anterior view. Using the computation of the fluid dynamic, the YF-SONATA's square back drag coefficient was calculated. The drag coefficient was 0.2461 which was a 20.64% reduction from the previous sedan type YF-SONATA. As mentioned the closed active air flap and covered flat bottom was applied in the design. Comparing the drag coefficient between the square back and a conventional sedan design, two types of YF-SONATA with only the active air flap and only full undercover design was considered. Computed fluid dynamic showed a 4.4% reduction of active air flap only, and a 4.1% reduction on the full under covered vehicle.[12,18]. Based on this research, combing these two models, assume no overlapping results, it comes out to an 8.5% reduction of aerodynamic drag and a 0.2837 drag coefficient result. Therefore, changing the design of the YF-SONATA square back produced sufficient outcome from the simulated models. A 0.2461 drag coefficient is a significant result.

Figure 4-11 through 4-12 show that stream line around the surface. Smooth streamline was detected without separation over the curvy roof. Also, weak downwash was observed because of the roof "kick-up" and the right angled side surface.

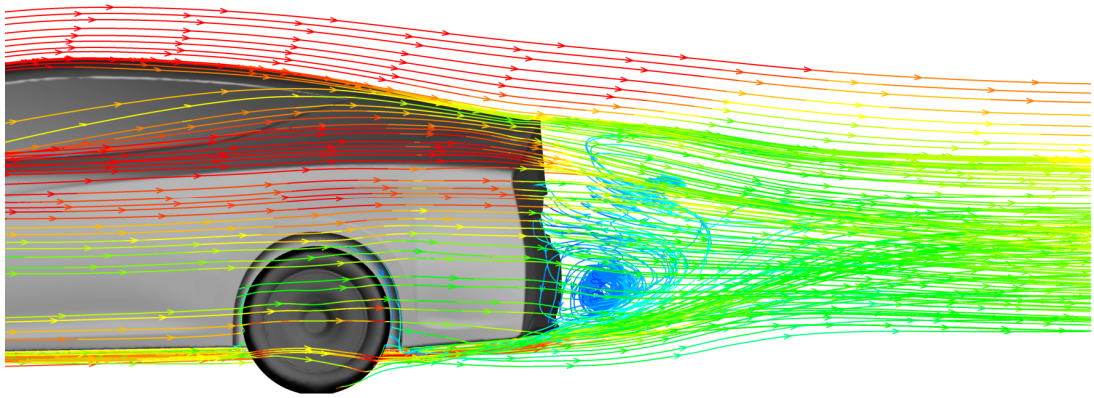

Figure 4-11. Streamline over the square back type vehicle (side angle)

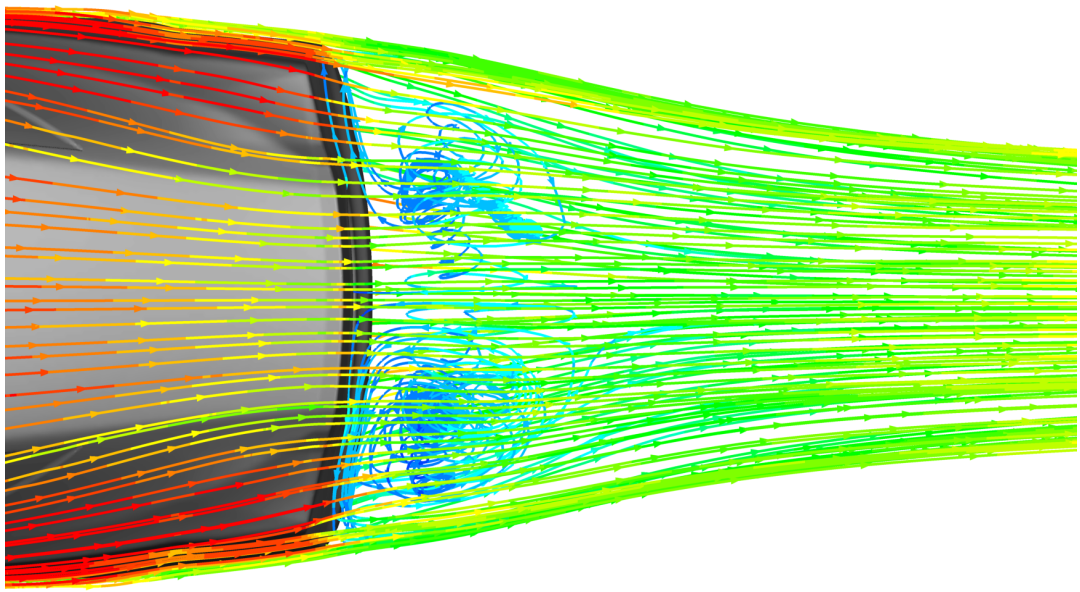

Figure 4-12. Streamline over the square back type vehicle (top angle)

Figure 4-13 is a surface pressure distribution at the centerline. Upper surface pressure distribution shows that the starting point of the front windshield has the highest pressure point and due to acceleration of the air, pressure decreases to the top of the vehicle. After that the pressure recovers depending upon decreasing surface elevation with decreasing air velocity. Lower surface pressure distribution shows that around the rear tire area indications of the lowest pressure and a recovering of the pressure passing through the diffuser.

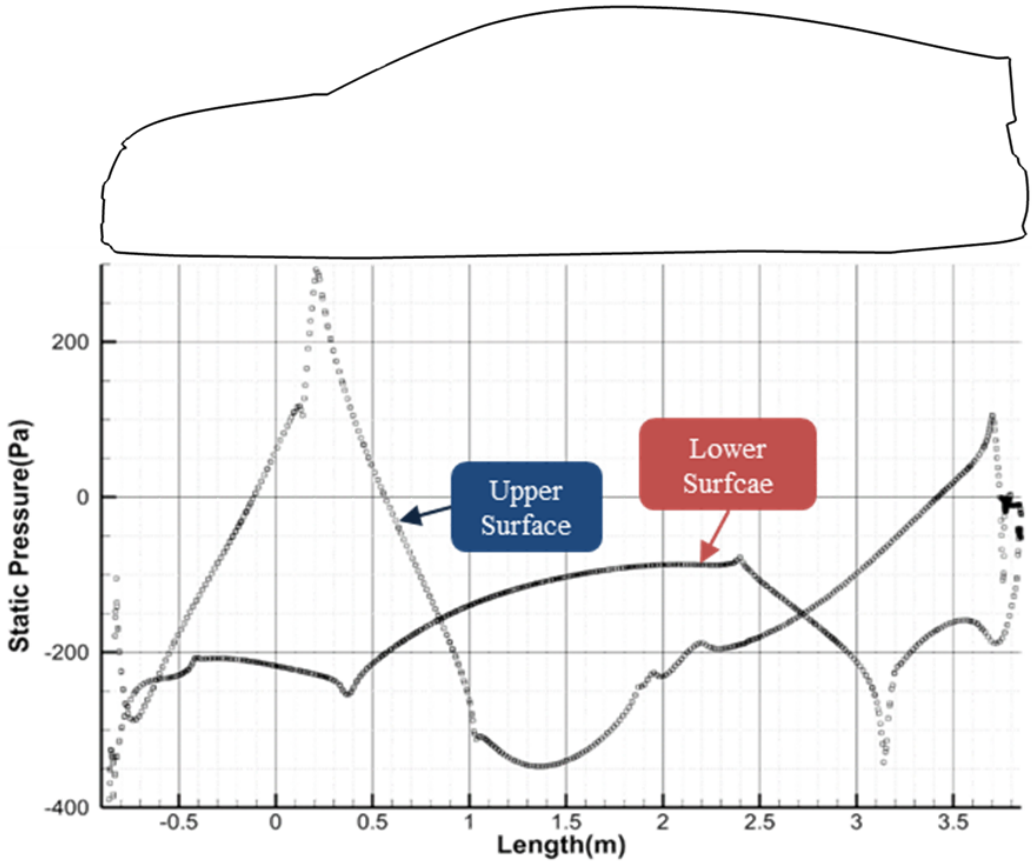

Figure 4-13. Pressure distribution of surface at centered line

3.4 Optimization of Square Back Rear Shape

3.4.1 Optimization Strategy

This study is defined as Single-Objective Optimization problem for minimizing the aerodynamic drag of the vehicle; objective function is drag coefficient. The Baseline of Optimization problem is the square back shape redesigned previously. Design variables of square back shape are roof angle, side angle, and diffuser angle. If there are many shape variables, sensitivity analysis is performed to observe sensitivity of shape variable about objective. But this step was skipped because there are few shape variables. Isight, a commercial optimization tool, is used for optimization process.

Constructing the sampling point, design of the experiment[55] was conducted using the Latin Hypercube Method(LHM)[56]. Through the Response Surface Model, the surrogate model was created to search the optimization of the square back shape. Due to finding the optimization point, the evolutionary algorithm, optimization algorithm has been used. Optimization process is below, as shown Figure 4-14.

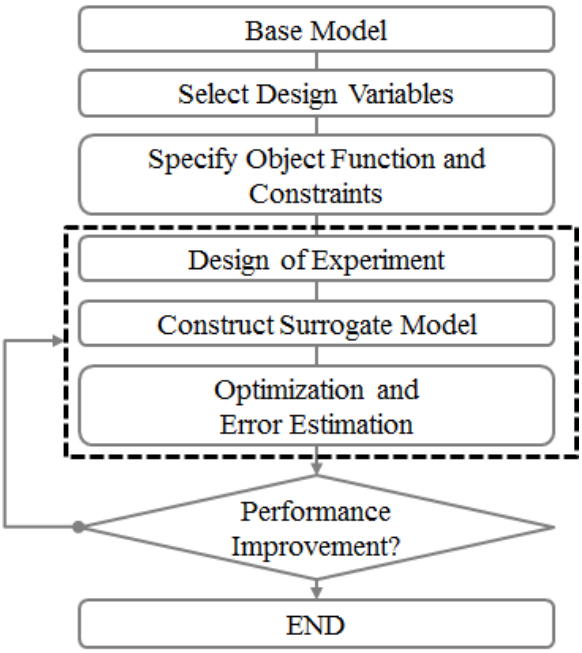

Figure 4-14. Optimization process

3.4.2 Design Variables

Roof angle, side angle, and diffuser angle, which are component of a square back shape, were selected by the design variables. These three variables are well known for highly affecting factors in the flow field around the vehicle. Figure 4-15 shows these three variables. Roof angle is defined as the angle between the extension of the horizontal line from the top of the vehicle and the end point of the roof line, which is a Baseline of 8 degrees. Diffuser angle is defined as the angle between the extension of the horizontal line from the starting point of the diffuser and the end point of the diffuser, which is a baseline of 5 degrees. The Side angle is applied with the same method as above. The baseline of the side angle is 7 degrees.

To prevent extreme deformation of the rear shape, the design space has been set. If the Roof angle is greater than 14 degrees, the edge of the roof collapses towards the body of the vehicle. So, the upper bound is set to be 14 degrees in order to prevent this kind of deformation. If the roof angle is less than 5 degrees, the edge of the roof erodes above the top of the roof line. So, the lower bound is set to be 5 degrees. If the Diffuser angle is lower than zero degrees, the end of the diffuser drops lower than the diffuser's lowest point. So, the function of the diffuser loses its purpose. Therefore, the lower bound is set to be 0 degrees and the upper bound is set to be 10 degrees. If the Side angle is less than 0 degrees, it protrudes beyond the side surface line. So, the lower bound is set to be 0 degrees. For the upper bound of the diffuser, the width of the square back type YF-SONATA has to be no less than 1560mm due to consideration of the conventional YF-SONATA trunk space allowance restriction: the measuring point of this width is 4570mm which is measured from the front to rear of the vehicle. If the side angle is greater than 14 degrees, the width of the vehicle gets narrower than 1560mm. The result, the maximum side angle is set to be 14 degrees. The baseline and range of variables are shown on the Table 4-1.

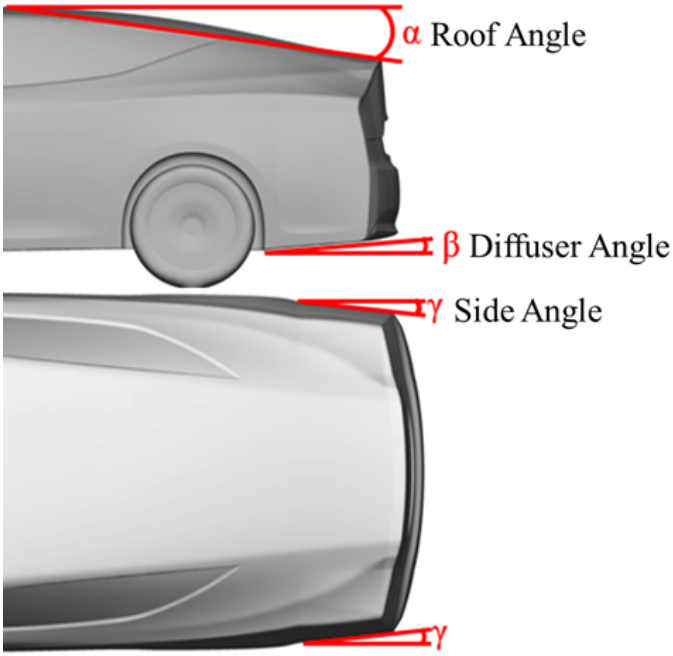

Figure 4-15. Design variables
: Roof angle, diffuser angle, and side angle

Table 4-1. Design variables and design space

Variables	Lower Bound	Baseline	UpperBound
Roof angle(α)	5°	8°	14°
Diffuser angle(β)	0°	5°	10°
side angle(γ)	0°	7°	14°

3.4.3 Design of Experiment

For design optimization, it is important to find the feasible design space formed by rages of design variables, which was determined based on preliminary sensitivity tests for the objective function in this work. Latin

Hypercube Method(LHM), which is an effective sampling method in the design and analysis of computer experiments[56], is a matrix of order $m \times n$ where m is the number of levels to be examined and n is the number of design variables. Each of the n columns of the matrix containing levels 1, 2, ⋯, m is randomly paired to form the Latin hypercube. LHM generates random sample points that ensure that all portions of the design space are represented. Using Latin Hypercube Method, 28 design points within the design space were selected including baseline as the design of experiment(DOE). computational analysis were performed about all design points. The result of design variable and objective are shown in Table 4-2.

Table 4-2. Results of design of experiment

α	β	γ	C_D	α	β	γ	C_D
8	**5**	**7**	**0.2461**	12	7	12	0.2230
9	5	10	0.2359	11	3	0	0.2528
11	8	14	0.2272	11	1	5	0.2389
13	3	6	0.2313	10	5	6	0.2388
8	9	13	0.2412	10	2	11	0.2314
12	9	9	0.2280	9	10	4	0.2526
12	4	12	0.2234	9	9	10	0.2387
6	2	8	0.2560	8	0	8	0.2437
5	7	10	0.2620	8	6	1	0.2619
11	7	4	0.2406	7	5	10	0.2471
7	6	5	0.2552	6	7	6	0.2629
8	10	7	0.2501	8	2	8	0.2428
14	4	3	0.2351	13	3	9	0.2266
13	9	7	0.2300	12	8	2	0.2434

3.4.4 Response Surface Model

The response surface model(RSM) was used to obtain the optimum design of the square back type YF-SONATA. Response surface modeling technique were originally developed to analyze the results of physical experiments to create empirically based models of the observed response values[59]. Response surface modeling postulates a model of the form

$$y(x) = f(x) + \epsilon$$

where $y(x)$ is the unknown function of interest, $f(x)$ is the polynomial approximation of x, and ϵ is random error that is assumed to be normally distributed with mean zero and variance σ^2. The error, ϵ_i, at each observation is assumed to be independent and identically distributed. The polynomial function, $f(x)$, used to approximate $y(x)$ is typically a low order polynomial, which is assumed to be either linear, Eq. (1), or quadratic, Eq. (2):

$$\hat{y} = \beta_o + \sum_{i=1}^{k} \beta_i x_i \tag{1}$$

$$\hat{y} = \beta_0 + \sum_{i=1}^{k} \beta_i x_i + \sum_{i=1}^{k} \beta_{ii} x_i^2 + \sum_{i=1} \sum_{j<1} \beta_{ij} x_i x_j \tag{2}$$

The parameters, β_0, β_i, β_{ii}, and β_{ij}, of the polynomials in Eqs. (1) and (2) are determined through least-squares regression, which minimizes the sum of the squares of the deviations of predicted values, $\hat{y}(x)$, from the actual values, $y(x)$. The coefficients of Eqs. (1) and (2) can be found using Eq. (3):

$$\beta = [X^{'} X]^{-1} X^{'} y \tag{4}$$

where X is the design matrix of sample data points, $X^{'}$ is its transpose, and y is a column vector that contains the values of the response at each sample point. Additional details on least-squares regression response surface modeling can be found in many books[58-60].

The RSM is constructed based on the evaluations of the objective functions at the prescribed design points. Figure 4-16 shows the relationship between the actual (simulated) and predicted (from the approximation model). The cross validation of the RSM was performed at every design point. This indicates confirmation about accuracy of the RSM. The Table 4-3 shows the result of R^2 and Root Mean Square Error(RMSE) value. When R^2 is closed 1, and RMSE is closed to 0, the response surface model will be more accurate. Based on the results of the cross validation, it is assured that numerical analysis and the RSM are valid and reliable.

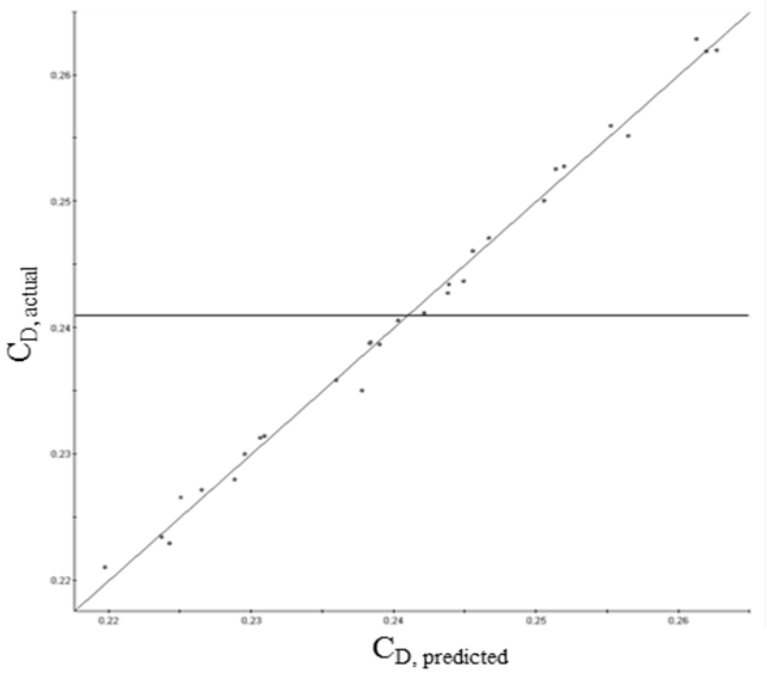

Figure 4-16. Accuracy of response surface model

Table 4-3. R^2 and RMSE of response surface model

	R^2	RMSE
Drag Coefficient	0.99344	0.02332

The Figure 4-17 through 19 show tendencies of objective to each design variable. The information about sensitivity of objective can be obtained. The drag coefficient tends to decrease according to increasing side angle and roof angle. The Figure 4-19 shows when roof angle gets larger, then drag coefficient gets smaller in the entire design space, and the diffuser angle, changing of angles 0 degrees to 10 degrees, has a tendency of decreasing in the beginning, but increasing when the angle gets larger. The diffuser angle which minimized the drag coefficient is determined by a specific roof angle. In this case, when the specified roof angle gets larger the diffuser angle gets larger in the same manner. The Table 4-4 shows the specific roof angle and diffuser angle indicating a minimum drag coefficient and drag coefficient values.

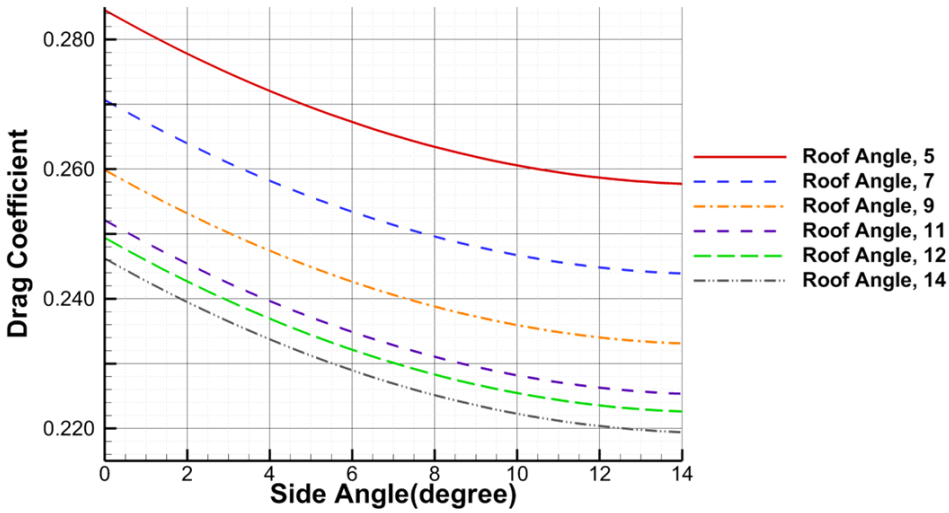

Figure 4-17. Relation between side angle and drag coefficient at diffuser angle is 5°

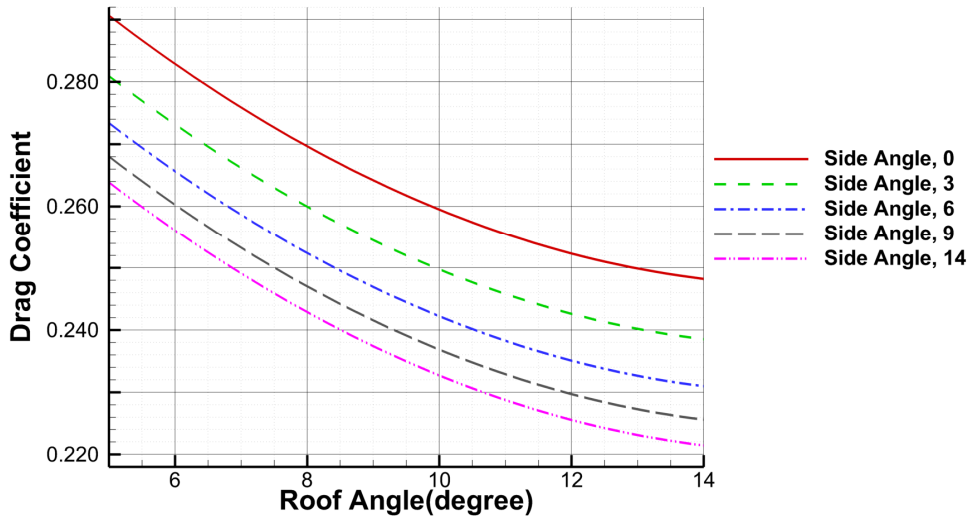

Figure 4-18. Relation between roof angle and drag coefficient at diffuser angle is 5°

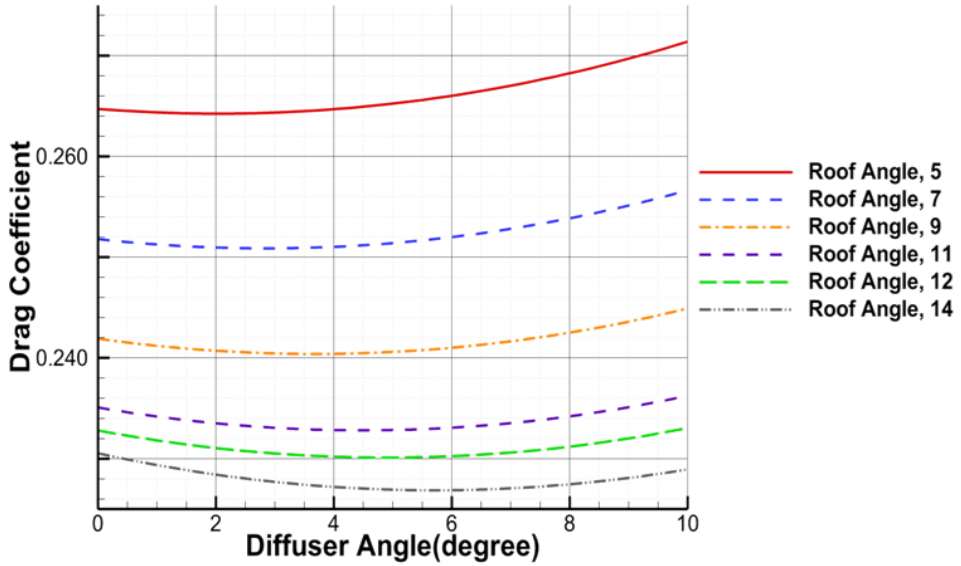

Figure 4-19. Relation between diffuser angle and drag coefficient at side angle is 7°

Table 4-4. Specific roof angle and diffuser angle indicating a minimum drag coefficient and its value.

Roof angle	5°	7°	9°	11°	12°	14°
Diffuser angle	2.04°	2.86°	3.67°	4.49°	4.9°	5.71°
Drag Coefficient	0.2642	0.2509	0.2404	0.2328	0.2301	0.2269

3.4.5 Optimization Result

Evolutionary Algorithms(EAs)[57] are emergent design optimization algorithms modeled on mechanism of the natural evolution. EAs search from multiple points, instead of moving from a single point. In addition, they require no derivatives or gradients of the objective function. These features lead to robustness and simplicity in coupling any evaluation codes. Parallel efficiency also becomes very high by using a simple master-slave concept for function evaluations, if such evaluations consume most of CUP time.Using Evolutionary Algorithm, optimization to minimize drag coefficient was performed in design space. Table 4-5 shows that optimization results. The results show that drag coefficient was predicted to be 0.219373 based optimization and improved by 10.85% compared to baseline. The drag coefficient was calculated to be 0.219354 by CFD analysis. Table 4-6 shows that the response surface model produced a good prediction with a relative error of 0.00866%. This represents that optimization using response surface model was reliable. Consequently, the drag coefficient of the optimum design represents a 10.85% improvement compared to the baseline. Comparison of baseline and optimal design shape was shown in Figure 4-20. Roof angle and side angle is larger than baseline and diffuser angle is almost similar to baseline. Roof angle and diffuser angle are 14° and 5.71°, respectively. This results are predicted from tendency between roof angle and diffuser angle which are set to specific roof angle and diffuser angle minimizing drag coefficient.

Table 4-5. Optimization result

		Baseline	Optimization
Objectve	Minimize C_D	0.2461	0.2194
Roof angle	α	8°	14°
Diffuser angle	β	5°	5.71°
side angle	γ	7	14°

Table 4-6. Validation of optimization result

	Prediction	Calculation	Error
Drag Coefficient	0.219373	0.219354	0.00866%

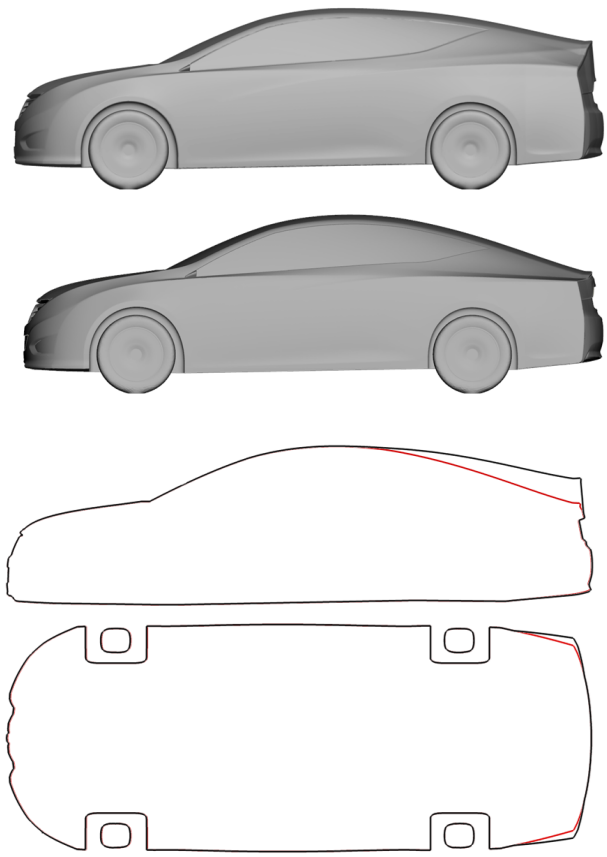

Figure 4-20. Comparison the shape lines of baseline and optimization result

The below Figure 4-21 compares the baseline and streamline of the optimal design. Figure to the left and right are streamline of the baseline and the optimal design. It can be seen that the re-circulation region of the optimal design became smaller compared to baseline. Decrease in the re-circulation region where pressure decreases indicates that the vehicle design was done appropriately to reduce the aerodynamic drag.

Figure 4-22 compares the surface pressure distribution of baseline and optimal design at the centerline. It can be seen that the surface pressure is increased at the diffuser area of the optimal design compared to baseline. The decreased pressure at the diffuser of the vehicle is one of the major factor to reduce the drag.

Figures 4-23 and 4-24 show the rear pressure distribution of the vehicle and pressure distribution with respect to the position on the rear surface. It can be seen that the rear pressure is entirely increased for the optimal design compared to that of baseline from Figure 4-23. The increased pressure past the diffuser affects the increase of pressure at the rear surface up to about 60 Pa as shown in Figure 4-24.

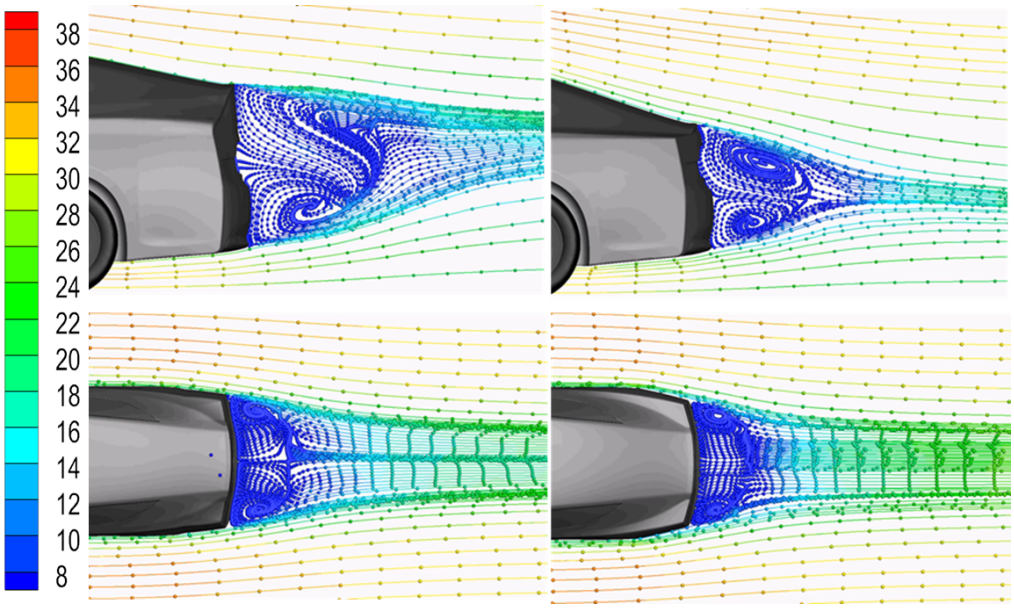

Figure 4-21. Comparison of baseline and optimal design streamline

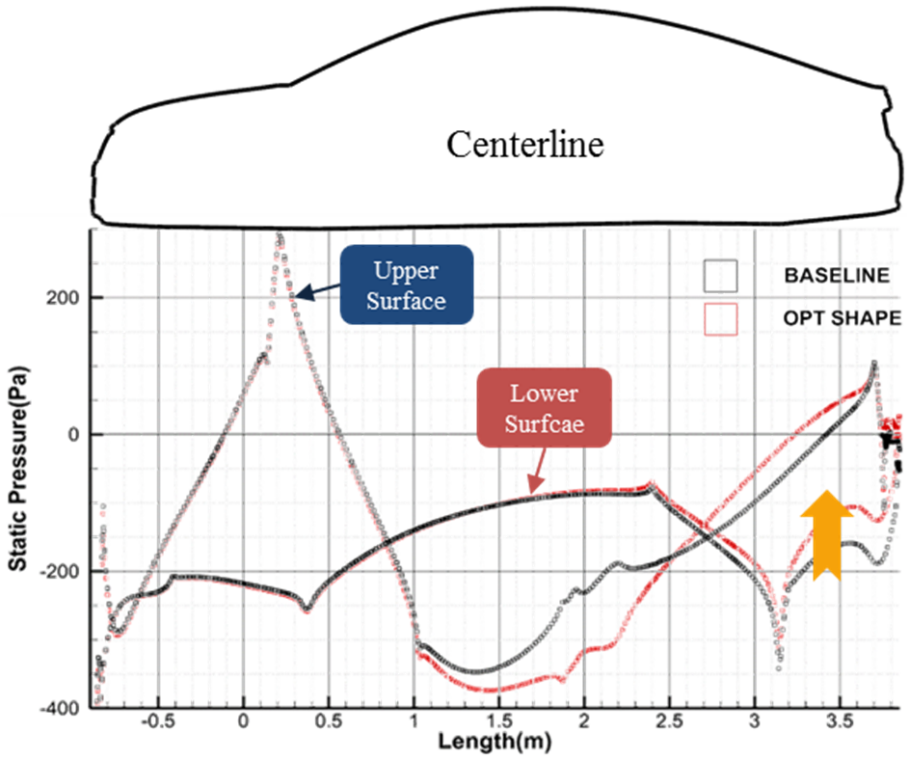

Figure 4-22. Comparison of surface pressure distribution on baseline and optimal design at centerline

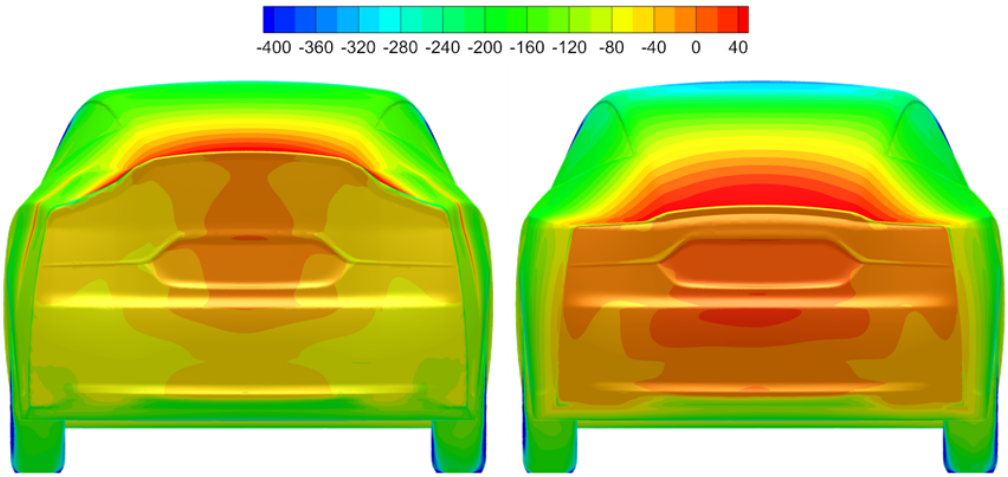

Figure 4-23. Comparison of surface pressure distribution on rear surface of vehicle(left : baseline, right : optimal design)

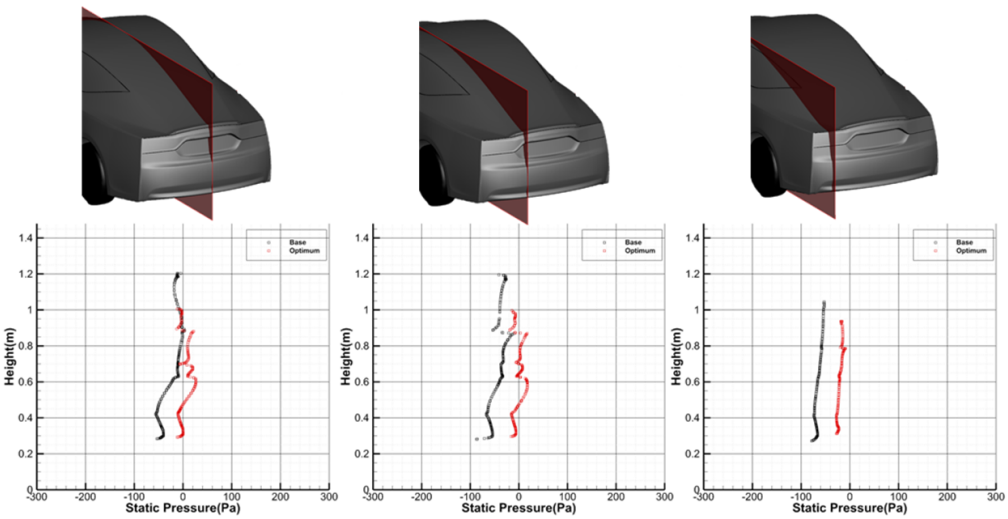

Figure 4-24. Comparison of pressure distribution with respect to the position on the rear surface(black : baseline, red : optimal design)

4. Installation of Aerodynamic Drag Reduction Devices

For reducing aerodynamic drag of vehicle, rear shape of sedan type YF-SONATA was redesigned to square back type. Then, rear shape of square back was optimized through optimization process. Through this process, drag coefficient of square back type YF-SONATA was improved by 29.25% compared to sedan type YF-SONATA. In order to futher improvement aerodynamic drag of vehicle, aerodynamic drag reduction devices were installed. Aerodynamic drag reduction devices are devices that control the external flow of vehicle, and the improvement about aerodynamic drag of vehicle has been proved by various researches[18,19,25,43,45]. In this study, side air dam, under deflector and wheel arch cover were installed to optimized design of square back type YF-SONATA and CFD analysis was performed as same as previous analysis.

4.1 Modeling

Side air dam was installed on under side of squareback type vehicle. Kim et al.[25] demonstrated that the height of side air dam is lower, the performance of side air dam is better. The limit of side air dam's height is minimum ground clearance which is 12 cm from the ground. Reflecting this result, side air dam that has a height from under the vehicle to ground and I shape was installed. Figure 4-25 show the modeling of side air dam shape.

Under deflectors are installed in front of the front wheels and rear wheels.

Under deflector have 3 cm height and rectangular shape. Under deflector in not rectangular shape rather it is curved inwards so that the device not only prevents the air flowing into the wheel housing but also reduce the obstruction to the flow.

The last installed aerodynamic drag reduction device is wheel arch cover. Wheel arch cover prevents fluid flowing the side of vehicle from flowing forward to rear wheel housing. It has a same height of side vehicle surface, connecting under parts to side air dam. This connection have a role of extension of side air dam. Wheel arch cover and under deflectors are shown in Figure 4-26.

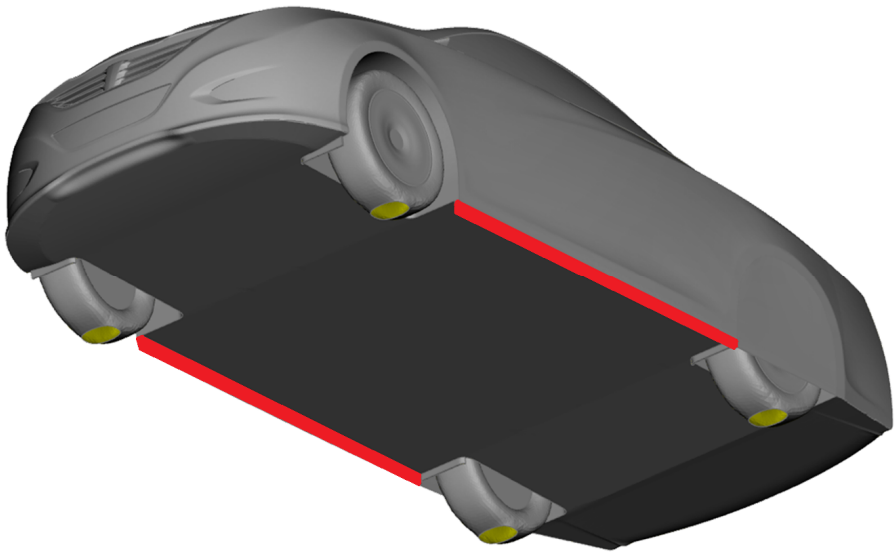

Figure 4-25. Installation side air dam

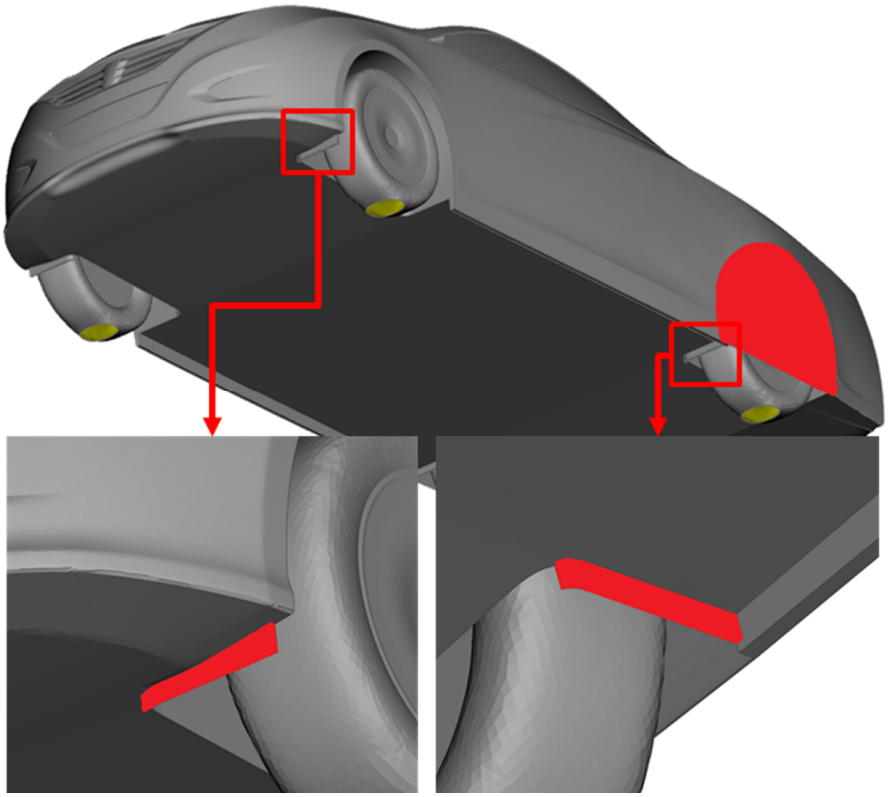

Figure 4-26. Installation wheel arch cover and under deflector

4.2 Flow Analysis Result

Drag coefficient of square back type vehicle that side air dam, wheel arch cover and under deflector was installed was predicted to be 0.2073 by CFD analysis. Aerodynamic performance was improved by 5.53% compared to vehicle having optimized square back shape. Aerodynamic drag distribution about each vehicle parts is shown as Table 4-7. Drag of vehicle surface is increased by . But wheel arch cover and under deflector prevent fluid to flowing toward wheels, so drag force acting on the front wheels and the rear wheels are considerably decreased. As decrement for aerodynamic drag acting wheels is bigger than increment for drag acting on vehicle surface, entire drag is improved. This result verified that aerodynamic drag reduction devices had an effect on the square back type vehicle. Table 4-8 shows that results from CFD analysis. Aerodynamic drag of optimial design of square back type YF-SONATA installed aerodynamic drag reduction devices was improved by 33.15% compared to sedan type YF-SONATA, which is base model in this study.

Table 4-7. Improve rate in accordance with installation of aerodynamic drag reduction devices

Drag Force(N)	optimal design of Square Back Type	optimal design of Square Back Type + Aerodynamic Drag Reduction Devices	Improvement Rate(%)
Vehicle Surface	291.87308	297.50201	-1.93
Front Wheels	28.124792	10.648466	62.14(Improved)
Rear Wheels	17.525934	9.706136	44.62(Improved)
Total	337.52381	318.85661	5.53(Improved)

Table 4-8. Results of improvement rate compared to sedan type YF-SONATA

	Drag Coefficient	Improvement Rate(%)	Remark
Sedan Type Vehicle	0.3101	-	Base
Baseline of Square Back Type	0.2461	20.64	
optimal design of Square Back Type	0.2194	29.25	
optimal design of Square Back Type + Aerodynamic Drag Reduction Devices	0.2073	33.15	

5. Conclusion

In this study, design of ultra-low aerodynamic drag vehicle was performed through optimization of rear shape and aerodynamic drag reduction devices. To reduce the aerodynamic drag, its rear shape was redesigned to square back type and optimization was performed. Aerodynamic drag reduction devices were installed to optimal design of square back type vehicle and drag coefficient was additionally decreased.

(1) Redesigning rear shape of sedan type to square back type

Rear shape of sedan type vehicle was redesigned to square back type which is widely known as having low aerodynamic drag. As a result of redesign of rear shape, aerodynamic drag was decreased by 20.64%.

(2) Square back rear shape optimization

Optimization was performed. The Baseline of Optimization problem is the square back shape redesigned. Roof angle, side angle, and diffuser angle were selected as design variables of square back shape, optimal design was searched through response surface model. As a result of optimization, aerodynamic drag was decreased by 10.85% compared to initial square back shape. This optimal design was decided to final model of square back shape.

(3) Installation of aerodynamic drag reduction devices

aerodynamic drag reduction devices(side air dam, under deflector, wheel arch cover) were installed to optimal design of square back type vehicle.

As a result of installing aerodynamic drag reduction devices, aerodynamic drag was improved by 33.15% compared to sedan type vehicle.

Aerodynamic drag was improved by 33.15% using optimization of rear shape and installation of aerodynamic drag reduction devices. 33.15% improvement of aerodynamic drag can be converted into 6.63% improvement of fuel efficiency and 20% reduction of vehicle's weight.

References

[1] Ju-Yong Lee, “Numerical Simulation on Flows in Engine Room With Various Exhaust of Engine Room Undercover,” MA Dissertation, Dep’t of Mechanical and Aerospace Eng., Seoul National Univ., 2011.02.

[2] Minho Lee, Jaehyuk Lim, Sungwoo Kim, Junghwan Kim, Kiho Kim, Choongsub Jung, “A study on the developments of vehicle fuel economy and CO2 emission correction formula according to the new test method,” KSAE, Spring Conference Proceedings, KSAE12-B0100, 2012.

[3] Shin-Kyung Lee, Doo-Seop Yun, Jeong-Woo Lee, Oh-Cheon Kwon, “A Study of Fuel and CO2 Exhaustion based on Vehicle Test,” KSAE, Spring Conference Proceedings, KSAE13-B0140, 2013.

[4] Se-Jun Kim, Seok-kee Shin, Kwang-Yeon Kim, “Study on the Vehicle Road-Load Affecting Factors,” KSAE 30th Anniversary Conference 2008 Proceedings, No 2, pp.803-809, 2008.

[5] Ki-Sun Song, Seung-On Kang, Hoon-Il Park, Jung-Do Kee, Kyu-Hong Kim, Dong-Ho Lee1, “External Flow Simulation Analysis of a Passenger Car for Drag Reduction,” KSAE, Fall Conference Proceedings, pp.1116-1125, 2010.11.

[6] Dae-Gyu Kim, Chul-Ho Kim, “A Numerical Study on the Aerodynamic Effect of a Front-side Air Deflector and Rear-side Shape of a Vehicle,” KSAE, Spring Conference Proceedings, KSAE13-B0358, 2013.

[7] Jeong-Jae Lee, Kyung-Ho Yoon, Chul-Ho Kim, “Optimum Aerodynamic Design of a Ultra-light Electric Vehicle to Maximize the Driving Distance,” KSAE, Spring Conference Proceedings, KSAE13-B0360, 2013.

[8] Je-Heon Kwon, Dae-Yeong Shim, Chul-Ho Kim, “A Numerical Study on the Aerodynamic Effect of a Streamlined Design of a High-speed Long-distance Bus,” KSAE, Spring Conference Proceedings, KSAE13-B0362, 2013.

[9] Doe Young Hur, Junguk Lee, Dongho Lee, “Aerodynamic Optimization on Conceptual Design Procedure of Ground Vehicle Design Process,”

KSAE, Fall Conference Proceedings, pp.707-710, 2011.11.

[10] Youjong Bae, Incheol Kim, Yongseok Shin, “A Development of the Active Air Flap System for Fuel Economy Improvement,” KSAE 2009 Annual Conference, pp.211-217, 2009.

[11] Tae-Kyung Kim, Ju-Yong Lee, Yeong-Bin Lee, Song-Ki Sun, Joon-Ho Lee, Dong-Ho Lee, Kyu-Hong Kim, “Numerical Simulation on Flows in 3-Dimensional Engine Room with Various Exhaust of Lower engine room,” KSAE, Spring Conference Proceedings, pp.657-667, May, 2011.

[12] Tae-Kyung Kim, Joong-Keun Choi, Jung-Hyun Kim, Jun-Ho Cho, Yeong-Bin Lee, Kyu-Hong Kim, Dong-Ho Lee, Jin-Phil Kim, Jun-Ho Lee, “Numerical Simulation of Flows and Aerodynamic drag with Active Air Flap in 3-Dimensional Engine Room,” KSAE, Spring Conference Proceedings, pp.452-462, May, 2012.

[13] Ju-Yong Lee, Tae-Kyung Kim, Yeong-Bin Lee, Dong-Ho Lee, Kyu-Hong Kim, “Numerical Simulation on Flows in 2-Dimensional Engine Room with various Exhaust of Lower engine room,” Proceedings of the 6th National Congress on Fluids Engineering, August, 2010.

[14] Yongkyu Lee, Jinil Park, Jonghwa Lee, Kyoungseok Park, Kwangyeon Kim, Junho Lee, “Vehicle Thermal Management by using Active Air Flap and Electric Cooling Parts,” KSAE, Spring Conference Proceedings, pp.197-200, 2012.

[15] Yongnyun Kim, Sunje Kang, Sukyung Kim, Woosung Kwon, Jongpaek Ha, “FEAF and Aerodynamics study to define front opening of mini vehicle in style development stage using Kriging method,” KSAE, Fall Conference Proceedings, pp.527-531, 2011.

[16] Chen-Guang Lai, Shigeru Obayashi, Yasuaki Kohama, Shinkyu Jeong, “Influence of the layout of engine-cooling outlet on automotive aerodynamic performance,” SNU-Tohoku Joint Workshop on Next Generation Aero Vehicle, Sep., pp.25-30, 2009.

[17] Bongha Song, Kyuik Lee, Jonpaek Ha, “Numerical analysis of Aerodynamic Drag of Engine Cooling Airflow,” KSAE, Spring Conference Proceedings, 2011.

[18] Tae-Kyung Kim, Seong-Min Jeong, Joong-Keun Choi, Kyu-Hong Kim, Jin-Phil Kim, Jun-Yong Lee, “Parametric Study of Aerodynamic Drag Reduction Devices for Aerodynamic Drag Reduction of Sedan(1) : Undercover and Under Fin,” KSAE, Spring Conference Proceedings, May, KSAE13-B0363, 2013.

[19] Tae-Kyung Kim, Seong-Min Jeong, Joong-Keun Choi, Kyu-Hong Kim, Jin-Phil Kim, Jun-Yong Lee, “Parametric Study of Aerodynamic Drag Reduction Devices for Aerodynamic Drag Reduction of Sedan(3) : Under Deflector,” KSAE, Spring Conference Proceedings, May, KSAE13-B0365, 2013.

[20] Ki-Sun Song, Seung-On Kang, Hoon-Il Park, Jung-Do Kee, Kyu-Hong Kim, Dong-Ho Lee, “Study on the Influence of Wheel Arches, Wheels, and Side Mirrors on Aerodynamic Performance of a Fast Cruising Passenger Car,” Transactions of KSAE, Volume 20, Issue 5, pp.26-35, 2012.

[21] Hyun Ho Park, Hyun Wook Han, Moon Sang Kim, Jong Paek Ha, Yong Nyun Kim, “A construction of wind noise analysis procedure and an analysis of wind noise around OSRVM based on the geometric parameter,” KSAE, Spring Conference Proceedings, pp.1695-1706, 2011.

[22] Hyun Ho Park, Hyun Wook Han, Moon Sang Kim, Jong Paek Ha, Yong Nyun Kim, “A Study on the Low Wind Noise OSRVM Shape Design using CFD,” KSAE, Spring Conference Proceedings, pp.1815-1827, 2011.

[23] Hyun Ho Park, Hyun Wook Han, Moon Sang Kim, Jong Paek Ha, Yong Nyun Kim, “A Study on the Optimized OSRVM Configuration for Improvement of Car Performance,” KSAE, Spring Conference Proceedings, pp.1736-1745, 2011.

[24] US Environmental Protection Agency, Retrieved 2013.04.05., http://www.epa.gov/smartway/technology/aerodynamics.htm

[25] Tae-Kyung Kim, Seong-Min Jeong, Joong-Keun Choi, Kyu-Hong Kim, Jin-Phil Kim, Kwang-Yeon Kim, “Parametric Study of Aerodynamic Drag Reduction Devices for Aerodynamic Drag Reduction of Sedan(2) : Side Air Dam,” KSAE, Spring Conference Proceedings, May,

KSAE13-B0364, 2013.

[26] Jin Hyuck Chang, Woo Gil Song, Jo Won Chang, “Study on Wake Structure and Aerodynamic Drag Reduction with Vehicle Shape Parameters,” KSAE, Fall Conference Proceedings, pp.1729-1735, 2011.

[27] Ki-Sun Song, Seung-On Kang, Hoon-Il Park, Jun-Ho Lee, Jung-Do Kee, Kyu-Hong Kim, Dong-Ho Lee, “A Parametric Study on the Effects of Rear Body Shape Modifications on Aerodynamic Performance of a 3D Passenger Car Represented by Vehicle Modeling Function,” KSAE, Spring Conference Proceedings, pp.732-741, 2011.

[28] Ki-Sun Song, Seung-On Kang, Sang-Ook Jun, Hoon-Il Park, Jung-Do Kee, Kyu-Hong Kim, Dong-Ho Lee, “Effects on Aerodynamic Drag Reduction of a Passenger Car by Rear Body Shape Modifications,” Transactions of KSAE, Vol 19, No 4, pp.137-145, July, 2011.

[29] Ki-Sun Song, Seung-On Kang, Sang-Ook Jun, Hoon-Il Park, Jung-Do Kee, Kyu-Hong Kim, Dong-Ho Lee, “Aerodynamic Design Optimization of Rear Body Shapes of a Sedan for Drag Reduction,” KSAE, Fall Conference Proceedings, pp.867-877, November, 2011.

[30] Ki-Sun Song, Seung-On Kang, Sang-Ook Jun, Hoon-Il Park, Jung-Do Kee, Kyu-Hong Kim, Dong-Ho Lee, “Aerodynamic Design Optimization of Rear Body Shapes of a Sedan for Drag Reduction,” International Journal of Automotive Technology, vol.13, no.6, pp.905-914, 2012.

[31] Seung-On Kang, Sang-Ook Jun, Hoon-Il Park, Yo-Cheon Ku, Jung-Do Kee, Kyu-Hong Kim, Dong-Ho Lee, “Aerodynamic Design Optimization of Automotive Vehicle Configuration Represented by Vehicle Modeling Function for Controlling COANDA Flow,” FISITA 2010 (World Automotive Congress), F2010B060, 2010.

[32] Seung-On Kang, Sang-Ook Jun, Hoon-Il Park, Yo-Cheon Ku, Jung-Do Kee, Dong-Hee Hong, Kyu-Hong Kim, Dong-Ho Lee, “Influence of Rotating Wheel and Moving Ground Condition to Aerodynamic Performance of 3-Dimensional Automobile Configuration,” Transactions of KSAE, Vol.18, No.5, pp.100-107, Sep., 2010.

[33] Seung-On Kang, Sang-Ook Jun, Hoon-Il Park, Yo-Cheon Ku, Jung-Do Kee, Kyu-Hong Kim, Dong-Ho Lee, “CFD Flow Simulation and

Aerodynamic Performance Prediction Around 3-D Automobile Configuration Represented by Vehicle Modeling Function," KSAE, Fall Conference Proceedings, pp.1306-1312, 2009.

[34] Hoon-Il Park, Young-Bin Lee, Seung-On Kang, Ki-Sun Song, Jung-Do Kee, Jun-Ho Lee, Hyoung-Seog Chung, Young-Il Jang, Kyu-Hong Kim, Dong-Ho Lee, "Experimental Studies on Aerodynamic Drag Reduction of a Passenger Car by applying Synthetic Jet," KSAE, Spring Conference Proceedings, pp.1130-1136, May 19th-21st, 2011.

[35] Hoon-Il Park, Young-Bin Lee, Jung-Uk Lee, Seung-On Kang, Kyu-Hong Kim, Dong-Ho Lee, "SHAPE OPTIMIZATION OF PIEZO-ACTUATED SYNTHETIC JET FOR ACTIVE FLOW CONTROL," Proceedings of the 6th National Congress on Fluids Engineering, August, 2010.

[36] Hoonil Park, Jun-Ho Jo, Jun-Ho Lee, Kyu-Hong Kim, Dong-Ho Lee, "Aerodynamic Drag Reduction of a Simple Bluff Body using Synthetic Jets," KSAE, Fall Conference Proceedings, pp.1995-1995, 2012.

[37] Hoonil Park, Jun-Ho Jo, Jun-Ho Lee, Kyu-Hong Kim, Dong-Ho Lee, "Drag Reduction of Simplified Car using Synthetic Jet Array," APAC-17 (Asia-Pacific Automotive Engineering Conference 2013), 2013.

[38] Hoonil Park, Jun-Ho Jo, Jun-Ho Lee, Kyu-Hong Kim, Dong-Ho Lee, "Parametric Study on Aerodynamic Drag Reduction of Simplified Car using Synthetic Jet Array," Journal of Mechnical Science and Technology, Accepted.

[39] Jun-Ho Cho, Seung-On Kang, Hoon-Il Park, Ki-Sun Song, Jung-Do Ki, Kyu-Hong Kim, Dong-Ho Lee, "Aerodynamic Drag Reduction of a Fast Cruising Passenger Car using Actively Translating Rear Diffuser Device," KSAE, Fall Conference Proceedings, pp.904-910, November, 2011.

[40] Seung-On Kang, Jun-Ho Cho, Sang-Ook Jun, Hoon-Il Park, Ki-Sun Song, Jung-Do Ki, Kyu-Hong Kim, Dong-Ho Lee, "Study of Active Rear Diffuser Device for Automotive Aerodynamic Drag Reduction," SAE Annual Conference, 2012.

[41] Seung-On Kang, Sang-Ook Jun, Hoon-Il Park, Ki-Sun Song, Jung-Do

Kee, Kyu-Hong Kim, Dong-Ho Lee, “Actively Translating Rear Diffuser Device for Aerodynamic Drag Reduction of Passenger Car,” International Journal of Automotive Technology, Volume 13, Issue 4, pp 583-592, 2012.

[42] Jun-Ho Cho, Seung-On Kang, Hoon-Il Park, Ki-Sun Song, Jung-Do Ki, Jun-Ho Lee, Kyu-Hong Kim, Dong-Ho Lee, “Influence of Active Translating Rear Diffuser Configuration to Aerodynamic Drag Reduction of Automotive Vehicle,” KSAE, Spring Conference Proceedings, pp.576-582, 2012.

[43] Tae-Kyung Kim, Seong-Min Jeong, Joong-Keun Choi, Kyu-Hong Kim, Jin-Phil Kim, Kwang-Yeon Kim, “Parametric Study of Aerodynamic Drag Reduction Devices for Aerodynamic Drag Reduction of Sedan(4) : Rear Diffuser,” KSME, Spring Conference Proceedings, May, 2013.

[44] Yongnyun Kim, Sunje Kang, Eunsoo Choi, “Aerodynamic Development of the Chevrolet Spark EV,” KSAE, Spring Conference Proceedings, KSAE13-B0359, 2013.

[45] Tae-Kyung Kim, Seong-Min Jeong, Joong-Keun Choi, Kyu-Hong Kim, Jin-Phil Kim, Jun-Yong Lee, “Parametric Study of Aerodynamic Drag Reduction Devices for Aerodynamic Drag Reduction of Sedan(5) : Active Air Flap, Undercover, Under Fin, Side Air Dam, Under Deflector and Rear Diffuser,” KSME, Spring Conference Proceedings, May, 2013.

[46] Van Doormal, J.P. And Raithby, G.D., “Enhancement of the SIMPLE Method for Predicting Incompressible Fluid Flows”, Numerical Heat Transfer, Vol 7, pp.147-163, 1984.

[47] Hashiguchi, M., Ihta, T. And Kuwahara, K., “Computational Study of Aerodynamic Behavior of a Car Configuration”, AIAA 19th fluid dynamics and Lasers Conference, pp.1-11, 1987.

[48] Rogers, Kwak, “Upwind differencing scheme for the time-accurate incompressible Navier-Stokes equations,” AIAA J. Vol. 28, No. 2, 1990, pp. 253-262

[49] Chang Sung Kim, “Sensitivity Analysis for the Navier-Stokes Equations with Two-Equation Turbulence Models and Its Applications,” Ph. D.

Dissertation, Dep't of Mechanical and Aerospace Eng., Seoul National Univ., 2001.

[50] Bo-Sung Lee, Dong-Ho Lee, "Parallel Computations on Steady/Unsteady Turbulent Flows around Two-Dimensional Transonic Airfoils," KAIA, 1998.

[51] Christopher L. Rumsey, Mark D. Sanetrik, Robert T. Biedron, N. Duane Melson, and Edward B. Parlette, "Efficient and Accuracy of Time-Accurate Turbulent Navier- Stokes Computations," AIAA 95-1835, June 1995.

[52] Andrea Arnone, Meng-Sing Liou, and Louis A. Povinelli, "Integration of Navier-Stokes Equations Using Dual Time Stepping and a Multigrid Method," AIAA J. Vol. 33, No. 6, 1995, pp. 985-990.

[53] Ansys 13.0 User Guide, Ansys Inc.

[54] W. H. Hucho, Aerodynamics of Road Vehicles from Fluid Mechanics to Vehicle Engineering, 4th Edition, USA, 1998.

[55] JMP, 2005, The Statistical Discovery Software, Version 6.0.0, SAS Institute Inc., Cary, NC.

[56] Sacks, J., Welch, W. J., Mitchell, T. J., and Wynn, H. P., 1989, "Design and Analysis of Computer Experiments," Stat. Sci., 4(4), pp. 409–423.

[57] Quagliarella, D., Periaus, J., Poloni, C., and Winter G. (Eds.), Genetic Algorithms in Engineering and Computer Science, John Wiley and Sons, Chichester, 1997.

[58] Myers, R. H., and Montgomery, D. C., Response Surface Methodology : Process and Product Optimization Using Designed Experiments, Wiley, New York, 1995.

[59] Box, G. E. P., and Draper, N. R., Empirical Model Building and Response Surfaces, Wiley, New York, 1987.

[60] Box, G. E. P., Hunter, W. G., and Hunter, J. S., Statistics for Experimenters: An Introduction to Design, Data Analysis, and Model Building, Wiley, New York, 1978.

국문 초록

본 논문에서는 차량의 후방형상 최적화와 공력저감장치를 통한 초저공력차량의 형상 설계에 관한 연구를 수행하였다. 현재 양산 중인 세단형 차량을 기본 형상으로 선택하였고, 후방형상을 저공력 형상으로 익히 알려진 스퀘어백 형상으로 재설계하여 공기저항의 감소 효과를 확인하였다. 스퀘어백 형상 설계는 공기역학적인 관점에서 이루어졌다. 새롭게 설계된 후방 형상을 대상으로 형상을 이루는 주요 변수들인 루프각, 사이드각, 디퓨저각을 설계 변수로 선정하여 항력계수(C_D)의 최소화를 목적함수로 한 최적설계를 수행하였다. 최적화 결과, 초기에 설계된 스퀘어백 형상 대비 약 10.85%의 공기저항이 개선되었고 설계 변수들이 차량의 공기저항에 미치는 상관관계와 공력특성을 파악하였다. 최적화된 스퀘어백 형상 차량의 공기저항은 세단형 차량에 비해 약 29.25% 개선되었다. 추가적인 공기저항의 감소를 위하여 최적화된 스퀘어백 차량에 공력저감장치인 사이드 에어댐, 언더 디플렉터, 휠아치커버를 설치한 후 항력 감소와 공력특성을 확인하였다. 이를 통하여 최종적으로 기본 형상인 세단형 차량 대비 33.15%의 공기저항을 개선하였다.

주요어 : 전산유체역학, C.F.D, 공기저항, 공력저감장치, 스퀘어백 형상 차량, 후방 형상 최적설계

학 번 : 2013-20722
이 름 : 최원석